Chapter 6: Effect Of The Development Of a Cell Barrier on Nanoparticle Uptake in Endothelial Cells

Abstract

In order to improve the current success of nanomedicine, a better understanding of how nano-sized materials interact with and are processed by cells is required. Typical in vitro nanoparticle-cell interaction studies often make use of cells cultured at different cell densities. However, in vivo, for their successful delivery to the target tissue, nanomedicines need to overcome several barriers, such as endothelial and epithelial cell barriers. Unlike sub-confluent or confluent cell cultures, cell barriers are tight cell monolayers, expressing a series of specialized tight junction proteins between adjacent cells to limit paracellular transport and ensure close cell-to-cell interactions. A clear understanding on how development of cells into a cell barrier may affect uptake of nano-sized drug carriers, is still missing. To this aim, here, human primary umbilical vein endothelial cells (HUVEC) are used as a model cell line to form endothelial cell barriers. Then, nanoparticle uptake is assessed in the developed endothelial barriers and compared to the uptake in sub-confluent or confluent HUVEC cultures. The results clearly show that the organization of cells into a cell barrier leads to a differential gene expression of endocytic markers, and – interestingly - this is accompanied by reduced nanoparticle uptake levels. Transport inhibitors are used to characterise the mechanisms involved in the uptake. However we show that some of them can strongly compromise barrier integrity, thus impairing the interpretation of the outcomes, and overall, only a partial inhibition of nanoparticle uptake could be obtained.

Valentina Francia,[†a] Aldy Aliyandi[†a] and Anna Salvati [*a]

[a]Groningen Research Institute of Pharmacy, University of Groningen, Antonius Deusinglaan 1, Groningen, 9713AV, The Netherlands.

[†] Valentina Francia and Aldy Aliyandi contributed equally to this work.

Manuscript in press, Nanoscale, 2018, DOI: 10.1039/C8NR03171A

Keywords: endothelial cells; HUVEC; barrier; uptake mechanisms, nanoparticle

Background

Nano-sized materials have been shown to be promising tools as drug carriers for the delivery of drugs, proteins and siRNAs because of their ability to exploit cellular mechanisms to be internalized by cells.[1–6] In particular nanomedicines have drawn a lot of interest for their potential as cancer therapeutics.[7] Nano-sized carriers can in fact be used for passive targeting because of their capacity to reach the tumor tissue via the so called enhanced permeation and retention (EPR) effect.[7–10] At the same time, they can also be decorated with targeting moieties and be directed specifically to tumors via active targeting. However, the presence and efficacy of EPR in humans is currently being debated[11–13] and recent debates have pointed out the - sometime - limited targeting efficiency of nanomedicines.[14–17] This has been accompanied by a growing realization that a better understanding on how nano-sized carriers are recognized and processed by cells could help improving further nanomedicine design for a more effective targeting.[18–20]

In order to reach their target, nano-sized carriers and drugs need to overcome a series of barriers both at organ, tissue and cellular levels.[21–23] Among these, endothelial cells constitute one of the very first barriers that nanomedicines need to overcome in order to reach the targeted organ following administration into the blood stream.[24,25] In order to control access to the underlying tissue and impair the passage of pathogens and undesired molecules, endothelial cells are typically organized in cellular barriers expressing tight junctions among cells, and with a clear spatial and functional separation between their apical and basolateral membranes.[26] As a result, endocytic pathways are differentially expressed between the two sides of the cell monolayer.[27] In order to reach the underlying tissue, nano-sized drug carriers may be able to use paracellular transport (if the barrier integrity is compromised or if specially designed to do so)[28,29] or – more often - they need to enter the cells by using the pathways expressed on the apical membrane and later be transcytosed from the basal membrane.[30,31] Other pathways that drugs can use to cross barriers may include specific transport proteins for smaller molecules, or simple diffusion across the cells for small lipophilic compounds. Overall, transport of (larger) nano-sized drug carriers across the endothelium is particularly challenging in the case of specialized endothelial barriers protecting organs such as - for instance - the brain, where the blood brain barrier constitutes a well-known example of one of the tightest barriers to drug delivery.[32–35]

Because of all of these reasons, organized cell layers expressing tight junction proteins may constitute *in vitro* models that better reflect the barriers nanomedicines encounter *in vivo* in comparison to cells at different degrees of confluency, which are often applied for nanoparticle cell behaviour studies.[6,18,36,37] Examples of nanoparticle studies using cell barriers are found in literature, especially for epithelial cells, such as for instance the skin,

intestine, lung and liver hepatocytes.[38–40] Less examples can be found in the case of endothelial cells, often focused on the endothelial blood brain barrier,[35,41] but not only.[40,42]

In general, optimizing cell culture conditions for ensuring the *in vitro* development of an intact cell barrier, without gaps among cells, can be particularly challenging.[41] In some cases it has been observed that the development of a cell barrier is accompanied by reduced nanoparticle uptake levels, for instance in epithelial cell barriers.[40,43–46] In the case of endothelial cells, however, a clear view on the effect of the development of a cell barrier on nanoparticle uptake and the cellular mechanisms involved is still missing.

Within this context, the aim of this study was to investigate how the differentiation of cells into a cell barrier *in vitro* affects nanoparticle uptake and behaviour in endothelial cells. For this purpose, we have chosen primary HUVECs (Human Umbilical Vein Endothelial Cells) as model (non-specialized) endothelial cells to develop endothelial cell barriers.[47] Several nanoparticle cell interactions studies have already used this as a model endothelial cell line,[48,49] including some examples in which cells were developed into barriers.[50–52] After carefully optimizing cell culture conditions to ensure proper formation of a cell monolayer expressing tight junction proteins, we tested the effect of barrier formation on the uptake of 50 nm amorphous silica as a representative model nanoparticle.[53] Thus, nanoparticle uptake kinetics in the barriers was directly compared to that in sub-confluent and confluent cells. Finally, protocols to use common chemical inhibitors of endocytosis on the cell barriers were carefully optimized with appropriate controls, paying special attention to the effect of these compounds on barrier integrity. The optimized protocols were then used for a preliminary study on the endocytic mechanisms involved in the uptake of 50 nm silica in the endothelial cell barriers.

Results and discussion

HUVEC barrier characterization and optimization

HUVEC cells were chosen as a model system to develop endothelial cellular barriers. Prior to nanoparticle studies, extensive work was performed in order to optimize the culture conditions for the development of a cell barrier expressing tight junction proteins. Different coatings such as rat tail collagen type-I or type-3 and 4, gelatin and fibronectin are typically used to improve adherence and growth of cells, including endothelial cells and HUVECs.[35,41,54–56] Rat tail collagen type-1, fibronectin and gelatin were tested and, as expected, they all allowed increased HUVEC adherence in comparison to uncoated surfaces, but with no obvious differences among them (see example in Supplementary Figure S1, for collagen type-1). Thus, we selected rat tail collagen type-I (as in many other studies with endothelial cells)[35,41] for further optimization of cell growth conditions.

Trans-Epithelial Electrical Resistance (TEER), permeability assays and imaging of tight junctions were combined in order to monitor the development of cell barriers in the different conditions tested (Figure 1 and Supplementary Figures S2-S8). As a first step, the barriers formed after seeding HUVECs at different starting cell densities (3000 and 50000 cells cm^{-2}) were compared. Imaging of ZO-1 (zonula occludens-1) and CD31 (cluster of differentiation 31, also known as PECAM1, platelet endothelial cell adhesion molecule), two common tight junction proteins in endothelial cells, was used to monitor cell barrier development at different days after seeding.[26]

In the first days, tight junction proteins were distributed intracellularly all over the cell. Only 7 days after seeding 3000 cells cm^{-2}, or 4 days after seeding 50000 cells cm^{-2} tight junctions were clearly visible in the margins between cells (Figure 1a and Supplementary Figures S2 and S3), suggesting development of a cell barrier. 3D z-stack images at confocal microscopy clearly confirmed this (Supplementary Movie S1 and projection in Figure 1c). It is important to notice that light microscopy seemed to indicate cell confluency already at earlier times, when fluorescence microscopy showed that proper tight junctions were not formed yet. This indicates that confluency alone is not a good parameter to assess the development of a cell barrier. At later days after seeding, HUVECs started to overlap in multiple layers and detached dead cells were also visible (see later for further details).

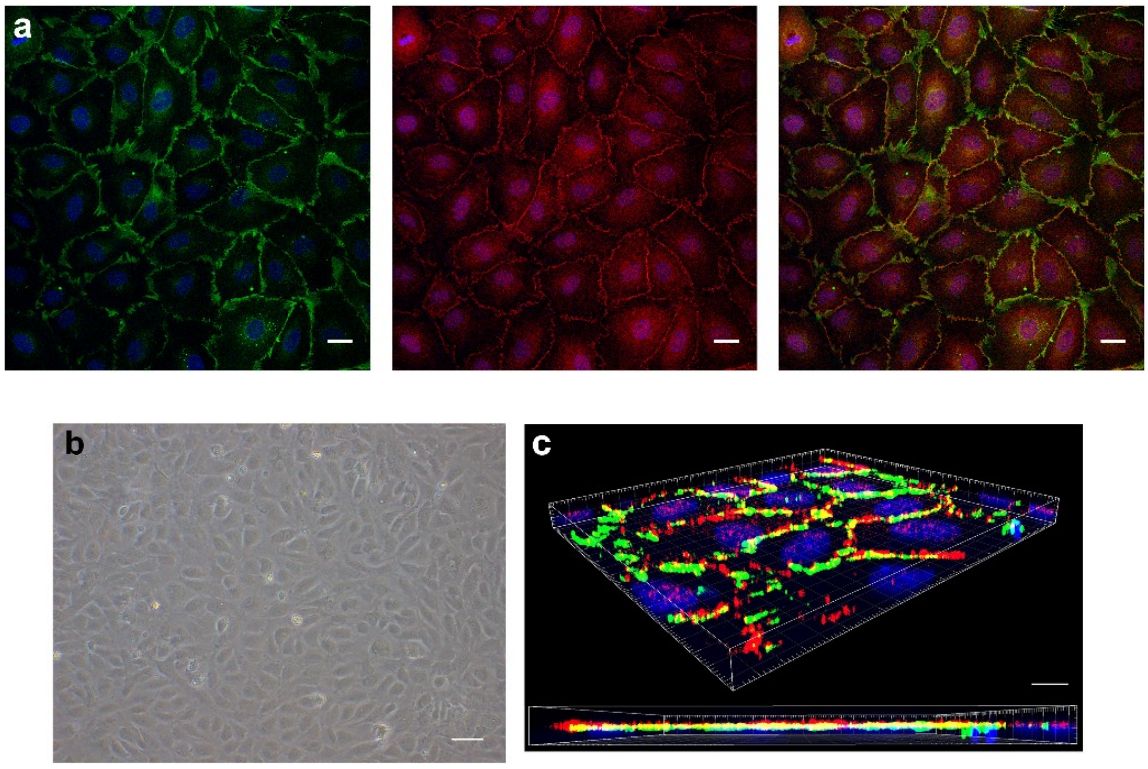

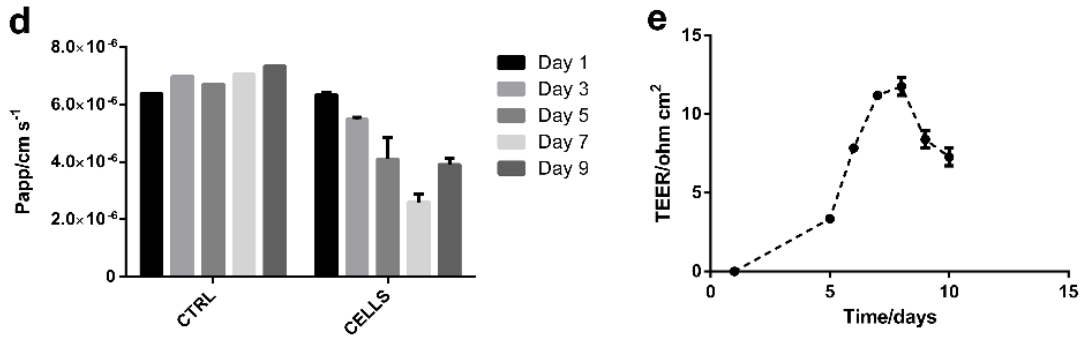

Figure 1. Characterization of the optimized HUVEC barriers. 3000 cells cm^{-2} HUVEC were plated on collagen coated glass coverslips (a-c) or Transwell inserts (d-e) and their growth was monitored for different days after seeding. **a and c**: confocal images of a HUVEC barrier (7 days after seeding) stained with anti-ZO-1 (red) or anti-CD31 (green) antibodies. Blue: DAPI stained nuclei. Scale bar: 20 µm. **b**: light microscopy image of the same culture. Scale bar: 50 µm. **c**: z- stack projection by confocal microscopy of a 7 day barrier (the corresponding movie is included in Supplementary Information). Scale bar: 10 µm. **d**: Apparent permeability (P_{app}) of FITC-Dextran (4 kDa, 200 µg ml^{-1}) at different times after seeding cells on polyester Transwell inserts. The fluorescence intensity of FITC-Dextran in the basal chamber was used to calculate the apparent permeability as described in the Experimental Section. Results are the average value and standard deviation of 2 different inserts. The results obtained with Transwells without cells are also included (CTRL). **e**: Trans Epithelial Electrical Resistance (TEER) at different times after seeding cells on polyester Transwell inserts. Results are the average TEER value and standard deviation obtained from two different inserts which were measured over time for the entire experimental period.

Trans-Epithelial Electrical Resistance (TEER) assays were also used to further characterize the development of cell barriers in the different conditions tested (Figure 1e and Supplementary Figure S4, including comparisons for barriers formed on filters of different materials). For this purpose, we selected 12 mm Transwell® inserts with a polyester filter of 0.4 µm pore size. Even though these measurements are very difficult to control quantitatively (see Supplementary Figure S5 as an example), the measured TEER values were comparable to what reported in literature for HUVECs in similar studies[57–59] and the trend observed was in all cases the same: TEER values increased as cell barriers formed in the first days after seeding, reaching a plateau roughly after 7-8 days or 2-4 days, for cells seeded at the lower and higher cell densities, respectively. These timescales are in agreement with what observed by imaging of tight junction proteins and light microscopy (Supplementary Figures S2 and S3). After that, for the lower cell density, the TEER values started to decrease, probably as a consequence of loss of barrier integrity and cell death (as clearly visible in light microscopy images before and after washing in Supplementary Figure S6, and also the fluorescence images of Figures S2). In the case of cells seeded at the higher cell density, after the plateau and a similar decrease, a second apparent peak in TEER could be observed. Also in this case, however, light microscopy images before and after washing the cell cultures (Supplementary Figure S7) showed strong cell death and compromised barrier integrity. This clearly excluded the possibility to interpret this second peak as an indication of an intact barrier (the observed formation of multiple cell layers in these overgrown barriers, as shown in Supporting Figure S3 day 9, may in part explain this second increase).

Overall, the TEER results showed that by starting with a lower cell density (3000 cells cm^{-2}) and waiting longer for barrier development, slightly higher TEER values could be obtained, suggesting a better barrier development in these conditions (Supplementary Figure S4).

The apparent permeability (P_{app}) of 4kDa FITC-Dextran across the developing cell layer was also used to monitor the development of a cell barrier (Figure 1d and Supplementary Figure S4, with an example of a corresponding calibration curve in Supplementary Figure S8). The values obtained were comparable with what was determined in literature for similar systems.[60–63] The results indicated that when 3000 cells cm^{-2} were seeded (Figure 1d), HUVEC permeability progressively decreased over time until 7 days after seeding, when it reached a minimum value corresponding to 40% of the permeability of a Transwell without cells (see also normalized results in Supplementary Figure S4c). Again, this timescale is comparable to what determined by TEER measurements and microscopy. On the other hand, the P_{app} of HUVECs seeded at high cell density (Supplementary Figure S4d) was already low since the beginning and fluctuated around the same values (40 to 60%) for all the experimental period (probably a smaller probe would be needed to be able to measure a decrease in apparent permeability in these conditions).

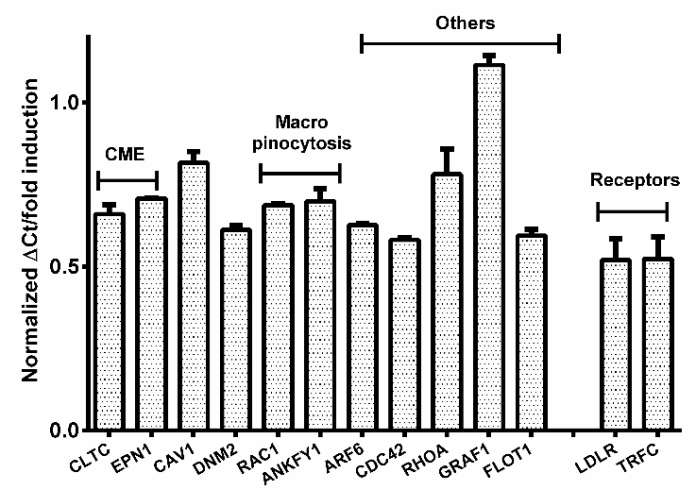

Figure 2. Expression levels of genes coding for endocytic proteins in HUVEC barriers in comparison to sub-confluent cells. HUVEC were seeded at a density of 3000 cells cm^{-2} and cultured for three or seven days. RT-qPCR was performed as described in the Experimental Section to determine the expression levels of genes coding for some cell receptors (LDL and transferrin receptors), and for a series of targets involved in clathrin mediated endocytosis (CME), caveolae-mediated endocytosis, macropinocytosis, and other clathrin and caveolae independent mechanisms (Others) (see also Supplementary Table S1 for details). Results represent the average and standard deviation over 2 replicates of the fold-change in gene expression levels in HUVEC barriers (day 7) compared to sub-confluent cells (day 3), calculated as detailed in the Experimental Section.

Taken all-together, tight junction staining, TEER and P_{app} assays suggested that seeding lower cell numbers and waiting for longer times allowed HUVEC to form tight junctions, which resulted in a high electrical resistance and a low permeability to molecules in about

7 days after seeding. We selected these optimized conditions for the following studies to assess the behaviour of nanoparticles on the developed cell barriers.

In order to test the effect of the development of a cell barrier on uptake and transport mechanisms, we also compared the expression levels of genes coding for key proteins involved in different endocytic pathways in sub-confluent HUVEC and in the optimized cell barriers (3 and 7 days after seeding 3000 cells cm^{-2}, respectively). Similar approaches were used to characterize an *in vitro* model of the blood brain barrier endothelium.[42] The results clearly showed that in all cases the mRNA expression levels of the selected endocytic targets were lower when cells were differentiated in a cell barrier compared to sub-confluent cells (Figure 2). Similarly, the gene expression levels of the same targets were also measured in confluent cells (25000 cells cm^{-2} seeded one day before the experiment). Cell counting confirmed that cell numbers in these confluent layers were comparable to the cell numbers in the optimized cell barriers (7 days after seeding 3000 cells cm^{-2}) (Supplementary Figure S9). Also in this case, the results showed that the gene expression levels of the selected endocytic targets were lower when cells were developed into a cell barrier (Supplementary Figure S10). Overall, this further confirmed that the optimized protocols allowed us to obtain a well-differentiated endothelial cell barrier. At the same time, the results clearly indicated that cell confluence alone does not guarantee the development of a cell barrier.

Nanoparticle uptake by HUVEC barriers

Having observed reduced expression of genes coding for key endocytic proteins in the optimized endothelial cell barriers, we then studied eventual consequences for nanoparticle uptake. This was done by directly comparing nanoparticle uptake levels in the optimized cell barriers and sub-confluent or confluent HUVEC cultures. To this aim we used red fluorescently labelled 50 nm silica as a well characterized model in nanoparticle uptake studies.[53] It is well established that once nanoparticles are dispersed in biological fluids, biomolecules from the surrounding environment adsorb on their surface, forming the so called nanoparticle corona.[47,53,64] More recently, it has also emerged that cell receptors can recognize and interact with the proteins adsorbed in this layer.[65–67]

Thus, in order to use a more relevant biological media for exposure to human endothelial cells, the nanoparticles were dispersed in a cell culture medium supplemented with human serum rather than the usual FBS. The use of a medium with human serum during exposure to the nanoparticles did not cause any major effect on cell viability and barrier integrity, in comparison to barriers maintained in standard FBS supplemented medium (data not shown). Dynamic Light Scattering was used to confirm that stable dispersions could be obtained in the conditions used for exposure to cells for up to 24 hours (see Supplementary Figure S11, after 24 hours incubation at 37 ˚C, 5% CO_2 in cell culture medium supplemented with human serum, HS EBM-2).

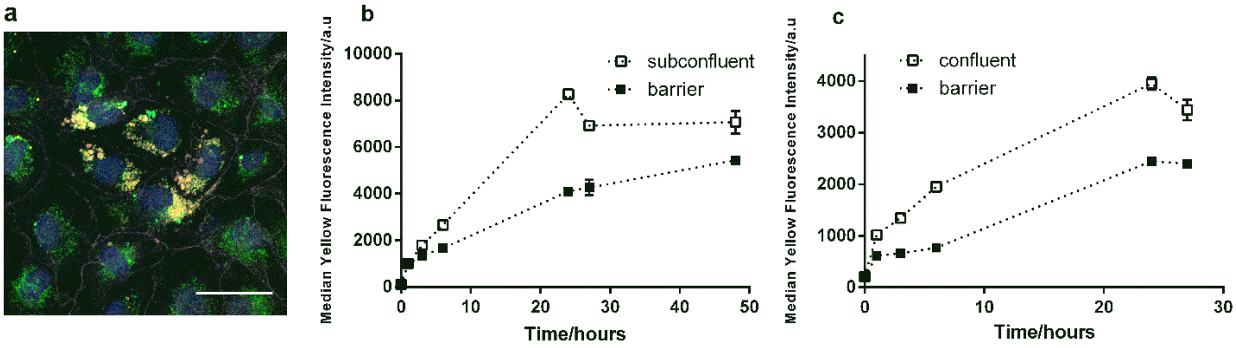

Figure 3. Nanoparticle uptake and intracellular trafficking in HUVEC barriers. **a:** confocal microscopy image of a HUVEC barrier (seven days after seeding 3000 cells cm^{-2}) exposed for 24 hours to 100 µg ml^{-1} 50 nm red SiO_2 nanoparticles. Red: nanoparticles, Green: LAMP-1, Grey: ZO-1, Blue: DAPI stained nuclei. Scale bar: 50 µm. **b-c:** Median cell fluorescence intensity as obtained by flow cytometry of HUVEC exposed for increasing times to 100 µg ml^{-1} 50 nm red SiO_2 nanoparticles dispersed in EBM-2 medium supplemented with 4 mg ml^{-1} human serum. Uptake levels in HUVEC barriers (seven days after seeding 3000 cells cm^{-2}) are compared to those in (b) subconfluent HUVEC (three days after seeding 3000 cells cm^{-2}) and (c) confluent HUVEC (one day after seeding 25000 cells cm^{-2}). The results are the average median fluorescence intensity of three replicates and error bars (included for all data points) are the standard deviation.

A direct comparison of nanoparticle uptake levels obtained in independent experiments, performed using same batches of nanoparticles and serum, confirmed good control and reproducibility of both the model cell barriers, as well as of the nanoparticle dispersions and exposure to cells (Supplementary Figure S12). As expected, the cell fluorescence intensity increased with incubation time as a consequence of nanoparticle uptake. Confocal microscopy confirmed nanoparticle uptake in the cell barriers and, as previously observed in different cell types for the same material,[3,68] nanoparticle accumulation into the lysosomes (Figure 3a).

As a next step, we compared the uptake of silica nanoparticles on sub-confluent cells and the optimized cell barriers (3 and 7 days, respectively, after seeding 3000 cells cm^{-2}) for up to 48 hours (Figure 3b). Interestingly, the results showed that nanoparticle uptake in the cell barriers was lower than in sub-confluent cells. In order to exclude that this was simply due to the higher cell number (thus lower dose of nanoparticles per cell) or to the lower surface area when cells are tightly packed into a barrier, we compared nanoparticle uptake in the cell barriers (7 days after seeding 3000 cells cm^{-2}) and in confluent cells with similar cell density (25000 cells cm^{-2} seeded one day before the experiment). As previously shown, cell numbers were comparable in the two conditions (Supplementary Figure S9). Also in this case, uptake in the cell barriers was lower than in confluent cells (Figure 3c). Importantly, the observed lower uptake was not unique to these specific nanoparticles, since similar results were obtained also with silica of bigger size (200 nm) and nanoparticles of a different material (carboxylated polystyrene of 40 and 200 nm) (see Supplementary Figure S11 for DLS characterisation, S13 for confocal microscopy and S14 and S15 for uptake studies). This result suggested that the lower uptake was not due to specific physico-chemical properties

of a particular nanoparticle type, rather depended on the development of cells into a cell barrier.

Nanoparticle uptake mechanism in HUVEC barriers

As a final step, we studied in more detail the mechanisms involved in nanoparticle uptake in the HUVEC barriers. The mechanisms that cells use to internalize nanoparticles still remain unclear in many cases, also because of the difficulty in characterizing transport pathways in cells and the limits of the different methods typically used to address this question.[18] RNA interference can be used to block selectively the expression of key proteins involved in different endocytic mechanisms, thus determining their role in nanoparticle uptake. However, it is known that primary cells, as also HUVEC, in most cases are very difficult to transfect and silence (see example in Supplementary Figure S16).[69,70]

For this reason, we used chemical inhibitors to block different uptake pathways thus determine their involvement in the uptake of the 50 nm silica nanoparticles (Figure 4). Chemical inhibitors are often used because they are relatively simple to use and their effect is very fast. However, it is known that their efficacy can vary in different cell types and they can also be very toxic, thus careful controls need to be performed in order to demonstrate their efficacy and exclude toxicity.[18,37] To this aim, protocols were optimized on the developed barriers by verifying the effect of the inhibitors on the uptake of control markers and by immunostaining of actin and microtubules. Eventual effects on barrier integrity were monitored by light microscopy (The results of the optimization studies for each of the compound tested are included in Supplementary Figures S17 to S21. Additionally, the results of Figure 4 after normalization for uptake levels in control cells without drugs are also given in Supplementary Figure S22).

Overall, HUVECs seemed to be particularly sensitive to all the drugs tested and most of the times the integrity of the cell barrier was impaired after exposure to the inhibitors (Figure 4), thus limiting the interpretation of the outcomes. With chlorpromazine, a compound commonly used to block clathrin mediated endocytosis (CME),[37,71] we obtained a decrease of only 30 to 50% at the different exposure times in the uptake of labelled low density lipoprotein (LDL), which is known to be internalized via CME (Figure 4a and normalized results in Supplementary Figure S22a). Furthermore, addition of chlorpromazine clearly resulted in loss of barrier integrity (Figure 4b), while lower drug concentrations were not effective in blocking the uptake of LDL (Supplementary Figure S17a). Using these conditions, around 40% inhibition of 50 nm silica nanoparticle uptake was observed at all exposure times in the compromised barriers in the presence of chlorpromazine (Figure 4c and normalized uptake results in Supplementary Figure S22b).

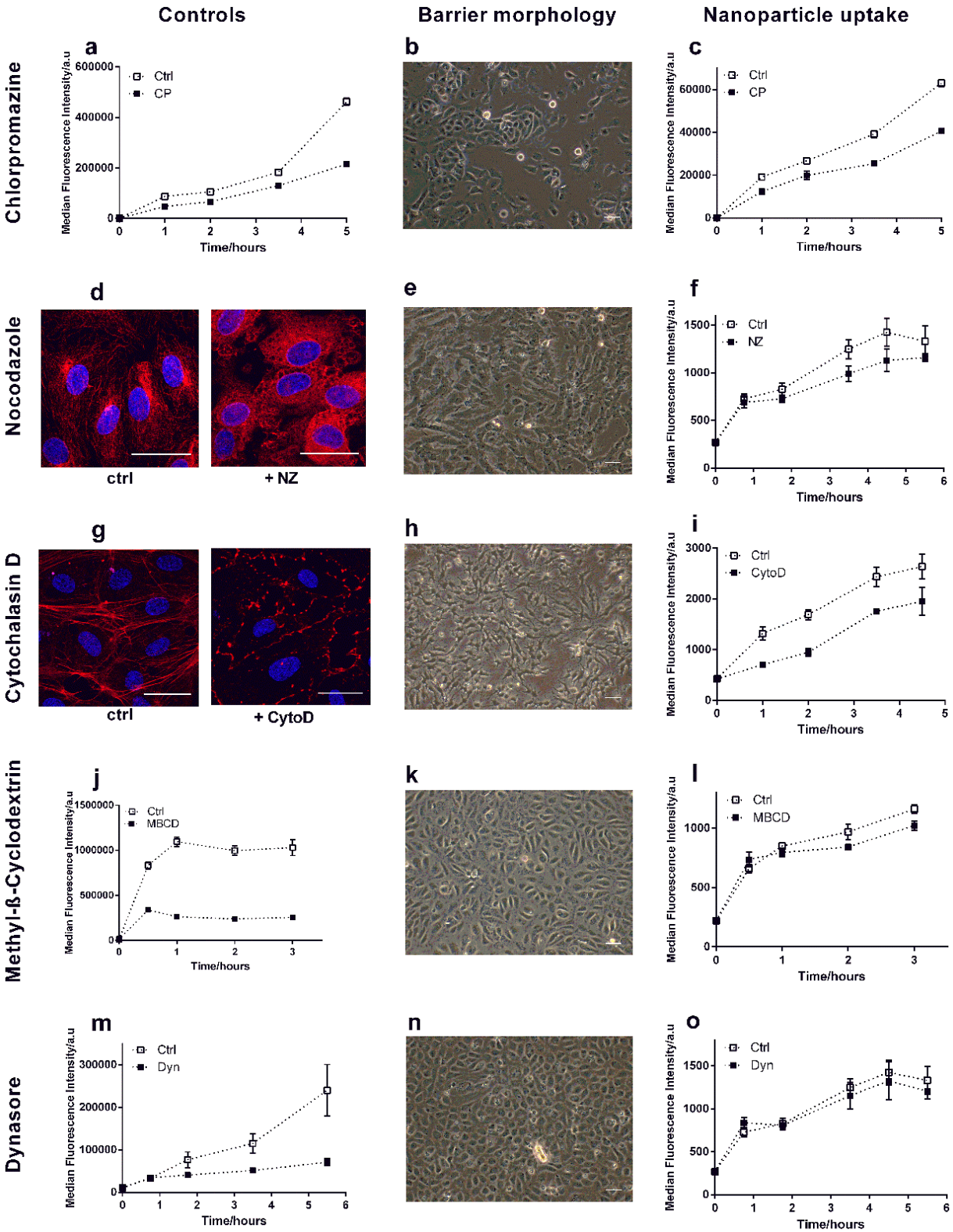
Controls
Barrier morphology
Nanoparticle uptake
Chlorpromazine
Nocodazole
Cytochalasin D
Methyl-ß-Cyclodextrin
Dynasore
a
b
c
d
e
f
g
h
i
j
k
l
m
n
o
Median Fluorescence Intensity/a.u
Time/hours
Ctrl
CP
NZ
CytoD
MBCD
Dyn
ctrl
+ NZ
+ CytoD

Figure 4. Uptake mechanisms in HUVEC barriers. HUVEC barriers (seven days after seeding 3000 cells cm^{-2}) were exposed to 5 µg ml^{-1} chlorpromazine (CP) (a-c), 5 µM nocodazole (NZ) (d-f), 0.5 µg ml^{-1} cytochalasin D (CytoD) (g-i), 2 mg ml^{-1} methyl-β-cyclodextrin (MBCD) (j-l), or 30 µg ml^{-1} dynasore (Dyn) (m-o). Left panels: controls for drug efficacy: uptake by flow cytometry of 2 µg ml^{-1} BODIPY-LDL (a and m), and 1 µg ml^{-1} of BODIPY LacCer (j) in control cells (Ctrl) and cells exposed to chlorpromazine, dynasore and MβCD respectively; confocal images were used as positive controls for nocodazole and cytochalasin D after staining the cells with fluorescent antibodies against tubulin (d) or actin (g) (scale bar: 30 µm). Middle panels: light microscopy images of HUVEC barrier morphology after exposure to each inhibitor (scale bar: 50 µm). Right panels: effect of the drugs on nanoparticle uptake. HUVEC barriers were exposed to 100 µg ml^{-1} 50 nm red SiO_2 nanoparticles in EBM-2 supplemented with 4 mg ml^{-1} human serum for the indicated times in the presence or absence of the different drugs. Results are the average and standard deviation of three replicates. The same results after normalization for the uptake in control cells without inhibitors are given in Supplementary Figure S22.

Nocodazole and cytochalasin D were then used to block microtubule and actin polymerization, respectively: these drugs are used often as inhibitors of macropinocytosis, but microtubule and actin are known to play a role also in other pathways, including CME.[18,37] Immuno-staining confirmed that both drugs had strong effects on microtubule and actin polymerization (Figure 4d and 4g). However, as observed for chlorpromazine, also these drugs caused evident disruption of the cell barrier (Figure 4e and 4h). This is perhaps not surprising considering their effects on microtubules and actin, which are essential to maintain cell shape and structure. In these conditions, maximum 20% inhibition of 50 nm silica nanoparticle uptake was observed in the compromised barriers in the presence of nocodazole and 30 to 40% inhibition at increasing exposure times in the presence of cytochalasin D (Figure 4f and 4i, respectively and normalized uptake results in Supplementary Figures S22c and S22d).

Next, methyl-β-cyclodextrin (MβCD) was used to sequester cholesterol from the plasma membrane. Cholesterol depletion is often used to block caveolae mediated endocytosis, however, it has been shown to affect also several other pathways.[18] Uptake of fluorescently labelled lactosylceramide (LacCer), a common compound that requires cholesterol for its internalization,[37] was used to verify MβCD efficacy. As opposed to the other drugs tested, in this case we could optimize protocols to achieve a very strong inhibition of LacCer uptake without compromising barrier integrity (Figure 4k). With the optimized conditions, LacCer uptake was strongly reduced up to 80% when MβCD was added (Figure 4j and normalized uptake results in Supplementary Figures S22e) and this reduction was even stronger at longer exposure times. However, no or only maximum 20% reduction of 50 nm silica nanoparticle uptake was observed upon cholesterol depletion in the cell barriers (Figure 4l and normalized uptake results in Supplementary Figures S22f).

Finally, we optimized protocols to expose the cell barriers to dynasore, a drug that suppresses dynamin-dependent endocytic pathways by inhibiting the GTPase activity of dynamin.[72] With the optimized conditions, the uptake of LDL, which is known to require dynamin for its internalization, was reduced by up to 70% at increasing exposure times (Figure 4m and normalized uptake results in Supplementary Figures S22g). Importantly, also

in this case the cell barrier integrity was maintained (Figure 4n). However, exposure to dynasore had only a minor effect on the uptake of 50 nm silica nanoparticles (roughly 10-15% inhibition at all exposure times) (Figure 4o and normalized uptake results in Supplementary Figures S22h).

As a final step, the same compounds were tested also on confluent cells in order to investigate eventual differences in uptake mechanisms between the barriers and confluent cells (Supplementary Figure S23). The results showed that only with cytochalasin D a small reduction of uptake could be observed (around 25% at all exposure times, as shown in Supplementary Figure S23h and S23i) and similarly with chlorpromazine at the longer exposure times (around 25% after 5 hours, as shown in Supplementary Figure S23b and S23c). This may suggest that different mechanisms are involved in comparison to what observed in cell barriers. However, further studies need to be performed to fully clarify this, and new methods need to be developed to fully characterize uptake mechanisms, especially for the cell barriers.

In conclusion, the concentrations of the different drugs tested needed to be optimized in order to achieve a good inhibition without affecting barrier integrity. In several cases this was not possible and the barrier was strongly compromised by exposure to some of these compounds. Exposure to chlorpromazine, nocodazole and cytochalasin D resulted in loss of barrier integrity and a partial reduction of 50 nm silica nanoparticle uptake in the compromised barriers. In the case of MßCD and dynasore, instead, we could achieve an optimal inhibition of the uptake of control markers, while preserving barrier integrity. However, 50 nm silica uptake was essentially unaffected by the two treatments. The lower effect on nanoparticle uptake could also be related to the presence of proteins in solution during exposure to nanoparticles, which may limit drug efficacy due to protein adsorption. As for the other compounds, higher drug concentrations led to loss of barrier integrity, making it again very challenging to conclude on the applicability of these compounds and more in general on the uptake mechanisms in the barriers. Overall, the partial reduction of uptake observed with these compounds may suggest the involvement of multiple pathways. However, given the strong effects on barrier integrity, it is difficult to conclude whether the same mechanisms are actually involved in the uptake of these nanoparticles in the fully developed cell barriers. Given that on confluent cells the results were slightly different than what observed in the barriers, and only cytochalasin D gave a (smaller) reduction of nanoparticle uptake, one may also hypothesize that even though the barrier integrity is compromised, the cells do retain some different behaviour. However, the results clearly indicated that overall different methods need to be developed to study uptake mechanisms in cell barriers, thus to be able to fully address this kind of questions.

Conclusions

The aim of this study was to determine the effect of the development of cells into a cell barrier on nanoparticle uptake in endothelial cells in comparison to standard cell cultures at different degrees of cell densities as commonly applied for *in vitro* studies. Different methods have been combined to monitor cell growth and to optimize the development of HUVEC endothelial cell barriers, varying conditions such as the presence of a coating, and the starting cell density. Barrier formation was confirmed via TEER measurements, permeability assays and imaging of tight junction proteins in the different conditions tested. Interestingly, a change in the expression levels of genes coding for several endocytic markers was also observed with the optimized conditions, further confirming the development of a differentiated cell barrier.

Thanks to the optimized growth conditions, we could determine that the development of a cell barrier affects nanoparticle interactions with cells. In particular, we found that nanoparticle uptake was lower in the endothelial cell barriers than in sub-confluent cells. Importantly, this behaviour did not depend on the specific physico-chemical properties of a particular nanomaterial, since the same results was obtained with nanoparticles of different sizes and different materials. This suggested that the lower uptake was due to the development of cells into a cell barrier. Furthermore, the observed reduction of uptake was not simply due to the lower surface area of the cells in the barrier, since lower uptake was observed also in comparison to confluent cells of similar cell density. Importantly, these results also indicated that cell confluence alone does not guarantee the development of a cell barrier with proper tight junction expression.

Various examples in literature showed a reduction in the endocytic activity of endothelial and epithelial cell types after differentiation[74] or polarization.[75,76] Here we show that the organization of HUVECs in a cellular barrier, which results into lower expression of genes coding for different endocytic markers, can also influence nanoparticle uptake levels.

It is important to keep in mind that not only the gene expression levels, but also the amount and localization of receptors and endocytic proteins on the apical or basal membranes is known to be affected by barrier formation and this might be relevant for nanoparticle uptake routes in endothelial cells. Further studies (beyond the scope of this paper) should be performed to determine for instance if the observed lowered gene expression of endocytic targets is also accompanied by a different distribution of receptors on the apical membrane. Such effects could also explain the observed differences in nanoparticle uptake levels. Similarly, it would be interesting to study whether there is a link between the lowered gene expression and the partial reduction of uptake observed with the inhibitors. However, our results also clearly show that different methods need to be developed to study uptake mechanisms in cell barriers, thus also to be able to address similar questions.

Given the strong effect of the development of a cell barrier on nanoparticle uptake levels, other aspects could be further implemented to develop *in vitro* models that resemble more closely the endothelial cell barriers that nanomedicines encounter *in vivo.* For instance, improvements may include mimicking the extracellular matrix or adding myocytes and connective tissue, which are known to be fundamental in sustaining endothelial cells *in vivo*. The use of 3D cultures could further promote cell differentiation by allowing the formation of endothelial tubes.[77] Similarly, the addition of a microfluidic system mimicking the blood flow and the resulting shear stress on the cells are also known to affect the expression of endothelial cell receptors.[78] Nanoparticle-cell interactions and corona formation are also affected when nanoparticles are exposed to cells in flow conditions, as opposed to static cultures.[55,79–83] Similar vessel-on a chip devices are being implemented[84,85] and could provide useful insights in nanoparticle-cell studies, both for nanomedicine and nanosafety.

Finally, here we also optimized protocols to use chemical inhibitors on the developed cell barriers and performed preliminary studies to try to characterize the mechanisms involved in the uptake. However, we found that preserving barrier integrity with these compounds is not always possible and overall only a partial reduction of uptake of 50 nm silica could be obtained in the compromised barriers. This may suggest that multiple pathways may be involved. However, clearly, other methods need to be developed and combined in order to be able to fully elucidate this and characterize how nanoparticles enter in similar endothelial cell barriers.

Methods

Cell culture

Primary Human Umbilical Vein Endothelial Cells (HUVEC) from pooled donors (LONZA, Allendale, NJ, USA) were grown in standard cell culture flasks under standard conditions (37 °C, 5% CO_2) in Endothelial Basal Medium (EBM-2) supplemented with EGM-2 bullet kit (LONZA). All experiments were performed using cells from passage 2 to maximum 7 in order to limit cell senescence and loss of the primary cell characteristics. The medium was changed every 48 hours.

Trans-Endothelial Electrical Resistance (TEER)

Trans-Endothelial Electrical Resistance (TEER) measurements were performed in order to monitor the formation and integrity of the HUVEC cell barriers over time. HUVEC were seeded at a density of 3000 cells cm^{-2} or 50000 cells cm^{-2} on 12 mm Transwell® inserts (Corning, NY, USA) with a polycarbonate or polyester filter of 0.4 µm pore size. The filters were pre-coated with cold rat-tail collagen type-I (100 µg ml^{-1}) (Corning, NY, USA) for 1 hour at room temperature, washed three times with PBS and air-dried for 20 minutes before cell

seeding. As common in this kind of studies,[41] in order to keep equivalent conditions for cell growth, the same procedure was followed to pre-coat also the plastic and glass substrates required for flow cytometry and fluorescence microscopy (see below). The basal and the apical chambers were both filled with cell culture medium pre-warmed at 37 °C (1.5 and 0.5 ml respectively, for all experiments with Transwell inserts). In order to monitor the development of the cell barriers, the TEER was measured using an EndOhm-6 chamber and an EVOM2 Meter (World Precision Instruments, Sarasota, FL, USA) every day up to 10 days after seeding. The TEER values of a blank insert without cells (5-6 and 10-12 Ω for PC and PE filters, respectively) were subtracted from the obtained resistance values and the results were multiplied by the insert area (1.12 cm^2) (thus the final values are expressed as Ω cm^2). The measurement was performed on two inserts for each condition and was repeated at least two times for each insert. Results are the average and standard deviation over the two replicates.

Para-cellular Permeability Assay

In order to monitor cell barrier development, the leakage of a fluorescent probe (4 kDa FITC-Dextran, Sigma-Aldrich St. Luis, USA) from the apical to the basal chamber of the Transwell® systems was monitored over time. Briefly, 3000 cells cm^{-2} or 50000 cells cm^{-2} were seeded on 12 mm Transwell® inserts as described above. FITC-Dextran (200 µg ml^{-1} in complete cell culture medium) was added to the apical chamber in Transwells with cells, as well as Transwells without cells (controls, CTRL) and the chambers were kept at 37 °C, 5% CO_2. Every 20 minutes, 100 µl of medium was collected from the basal chamber and replaced with 100 µl of fresh medium for a total of 2 hours. The fluorescence intensity was measured immediately using a Gemini EM microplate spectrofluorometer (Molecular Devices, CA, USA) and the apparent permeability coefficient (P_{app}) of FITC-dextran was determined as described in literature[73] using the following equation:

$$\mathrm{Papp} = \frac{\Delta Q}{\Delta t \times A \times C} \qquad (1)$$

where $\Delta Q\ \Delta t^{-1}$ is the permeability rate (µg s^{-1}), C is the initial concentration of FITC-dextran in the apical chamber (µg ml^{-1}), and A is the surface area of permeable membrane inserts (cm^2). Serial dilutions of FITC-dextran in complete EGM-2 medium (in the range 0 to 25 µg ml^{-1}) were used to determine for each experiment a calibration curve of the fluorescence intensity as a function of concentration (see an example in Supplementary Figure S6). This was used to determine the transported mass ΔQ over the investigated time Δt, taking into account the medium replacement in the basal chamber. Normalized data were obtained by dividing the P_{app} obtained on Transwells with cells with that obtained on Transwells without cells (100% P_{app}).

Immunohistochemistry

Cell confluency and morphology were assessed regularly using light microscopy (Olympus IX50). Tight junction proteins were immunostained and their expression and distribution inside cells determined by confocal imaging. Briefly, 3000 cells cm^{-2} or 50000 cells cm^{-2} were seeded in a 24-well plate (Corning) on glass coverslips pre-coated with rat-tail Collagen Type-I as described above. At different days after seeding, cells were fixed with formaldehyde (4% v/v) solution for 15 minutes and permeabilized with Triton X-100 (0.1% v/v) for 5 minutes. Subsequently, cells were incubated with a polyclonal rabbit primary antibody against the tight junction protein ZO-1 (zonula occludens-1, Life technologies, NY, USA) and monoclonal mouse primary antibody against CD31 (cluster of differentiation 31, also known as PECAM1, platelet endothelial cell adhesion molecule, Dako, Glostrup, Denmark) for 1 hour at room temperature, followed by incubation in Alexa Fluor®488 goat anti-mouse (Life technologies, NY, USA) and Cy®5 goat anti-rabbit (Jackson Immuno Research Laboratories, Inc., PA, USA) secondary antibodies for 1 hour. The effect of nocodazole on microtubules was assessed by incubating samples with a mouse primary antibody against human α-Tubulin (Merck Millipore, Netherlands) for 1h followed by incubation with a Alexa Fluor®488 goat anti-mouse secondary antibody (Life technologies, NY, USA) for another hour. Efficacy of cytochalasin D on actin depolymerization was assessed by incubating samples with phalloidin conjugated with TRITC (Sigma-Aldrich St. Luis, USA), which stains F-actin selectively. After antibody incubation, cells were washed 3 times with PBS. Nuclear staining was performed by incubating cells for 5 minutes with DAPI (4',6-diamidino-2-phenylindole). Subsequently, slides were mounted with Mowiol 4-88 mounting medium (EMD Chemical, Inc., CA, USA). Images were taken using a Leica TCS SP8 fluorescent confocal microscope (Leica Microsystems, Wetzlar, Germany) with a 405 nm laser for DAPI excitation, a 488 nm laser for Alexa Fluor®488, a 552 nm laser of TRITC and a 638 nm laser for Cy5®. Images were processed using ImageJ software (http://www.fiji.sc). IMARIS V.7.6.4 software (Bitplane, St. Paul, MN) was used for 3D reconstructions of the z-stack images and to generate the corresponding movie. In order to increase the visual clarity of the 3D images, the brightness and contrast of the tight junction protein channels (ZO-1 and CD31) were adjusted.

mRNA expression

In order to determine the effect of barrier formation on cells, the expression levels of a series of genes coding for proteins known to be involved in different endocytic pathways were determined by RT-PCR using the primers listed in Table S1, Supplementary Information. HUVECs were seeded at a density of 3000 cells cm^{-2} and cultured for 3 or 7 days as previously described. Additionally, to measure expression levels in confluent cells, cells were seeded at a density of 25000 cells cm^{-2} and cultured for 1 day. Then, total mRNA was isolated using an Invitrap® Spin Cell RNA Mini Kit (Stratec Molecular GmbH, Berlin,

Germany) according to the instruction provided by the manufacturer. Reverse transcription of mRNA (2 µg for both day 3 and day 7 cultures) into cDNA was performed using a Reverse Transcription System (Promega, Leiden, The Netherlands) in an Eppendorf Mastercycler gradient (the following cycle was used: 20 ˚C for 10 min, 42 ˚C for 30 min, 20 ˚C for 12 min, 99 ˚C for 5 min and 20 ˚C for 5 min). The transcription levels were measured by quantitative real time PCR (SensiMix™ SYBR kit, Bioline, Taunton, MA) in a ABI7900HT sequence detection system (Applied Biosystems, Foster City, CA) from cDNA (20 ng per sample). The Ct values were obtained using a SDS 2.4 software (Applied Biosystems). For each target, 4 replicate wells were prepared and the average Ct value and its standard deviation were calculated. Results are expressed as fold-change of the averaged Ct values of day 7 samples (Ct_7) related to Ct values of control day 3 samples (Ct_3) as follows:

$$\text{Fold change} = 2^{-(\text{Mean } Ct_7 - \text{Mean } Ct_3)} \quad (2)$$

The same formula was used to calculate the fold-change of Ct values of day 7 barriers related to Ct values of confluent cells.

Nanoparticle characterization

Red fluorescently labelled (Maximum excitation and emission wavelengths 569 and 585 nm respectively) silica nanoparticles (SiO_2 nanoparticles) of 50 nm and 200 nm were purchased from Kisker Biotech (Steinfurt, Germany). Different batches (LOT numbers) of the same product were used among some of the different experiments presented. Fluorescently labelled red (580/605) and orange (540/560) carboxylated polystyrene nanoparticles (PS-COOH nanoparticles) of 40 nm and 200 nm – respectively - were purchased from Invitrogen (Life Technologies, Carlsbad, CA, USA). In order to characterize the nanoparticle dispersions and monitor their stability throughout the duration of the experiments, nanoparticle size distributions were measured using Dynamic Light Scattering (DLS) with a Malvern Zetasizer Nano ZS. The same instrument was used also to measure zeta potential (ζ-potential). Briefly, nanoparticles (100 µg ml^{-1}) were dispersed in PBS, dH_2O or the cell culture medium (EBM-2) supplemented with 4 mg ml^{-1} human serum (human serum from pooled donors, from TCS BioSciences Ltd Botolph Claydon, Buckingham, UK) at 20 ˚C and immediately measured, using disposable folded capillary cells (Malvern Instruments Ltd., Worcestershire, UK). Different batches of pooled human serum were used for some of the experiments presented. In order to monitor nanoparticle stability during exposure to cells, nanoparticles were incubated for 24 hours in complete culture medium in the same conditions as when exposed to cells (37 °C, 5 % CO_2). Size measurements were averaged results from 5 runs of at least 3 measurements.

Exposure to nanoparticles and flow cytometry analysis

Cell fluorescence intensity was used as a measurement of nanoparticle uptake in HUVEC at different days after seeding and on the fully developed cell barriers. HUVEC were seeded in

24-well plates at a density of 3000 cells cm^{-2} and grown for 7 or 3 days, as described above. Additionally, cells were seeded at a density of 25000 cells cm^{-2} and cultured for 1 day. Then, HUVEC were exposed for different time periods to 50 nm red SiO_2 (100 µg ml^{-1}), 200 nm red SiO_2 (200 µg ml^{-1}), 40 nm red PS-COOH (2 µg ml^{-1}) or 200 nm orange PS-COOH (3 µg ml^{-1}). Given the different nanoparticle size, density and fluorescence, different mass concentrations were selected for each nanoparticle type in order to ensure good fluorescence signals in cells. Nanoparticles were dispersed at room temperature in cell culture medium containing human serum (human serum from pooled donors, from TCS BioSciences Ltd Botolph Claydon, Buckingham, UK). The final serum concentration was 4 mg ml^{-1}, roughly corresponding to the protein concentration present in standard cell culture media prepared using 10% fetal bovine serum. Cells were exposed to the freshly made nanoparticle dispersions immediately after mixing, by replacement of the cell culture medium. In order to reduce variability due to the preparation of nanoparticle dispersions, cells were seeded and grown so that the same nanoparticle dispersion was used to incubate HUVEC which were grown for different days after seeding. After different exposure times, cells were washed with medium supplemented with FBS (10% v/v) and twice with PBS in order to remove nanoparticle excess and reduce the presence of eventual nanoparticles adhering outside the cell membrane. Thus cells were harvested using trypsin–EDTA (0.05% v/v). Cell fluorescence for nanoparticle experiments was recorded using a BD FACSArray (BD Biosciences, Erembodegem, Belgium) with a 532nm laser or – for the results in Figure 4c - using a Cytoflex Flow Cytometer (Beckman Coulter, Woerden, the Netherlands) with a 488 nm laser. Data were analyzed using Flowjo® data analysis software (Flowjo, LLC). Double scatter forward and side scattering plots were used to set gates in order to exclude cell debris and cell doublets and select intact cells. For each experiment, a total of at least 15000 cells were acquired per sample and each sample was performed in triplicate. The results in the Figures are expressed as the averaged median cell fluorescence intensity and standard deviation over the 3 replicates. At least 3 independent experiments were performed to confirm the results.

Cell counting

In order to determine the number of cells in confluent cultures and the optimized barriers, HUVEC were seeded in 24-well plates at a density of 3000 cells cm^{-2} and grown for 7 days, as described above. Additionally, cells were seeded at a density of 25000 or 50000 cells cm^{-2} and cultured for 1 day. Then, cells were harvested using trypsin–EDTA (0.05% v/v) as described above and cell numbers were counted using a Neubauer hemocytometer or by flow cytometry, using a Cytoflex Flow Cytometer (Beckman Coulter, Woerden, the Netherland. The instrument allows to determine the number of cells in calibrated volumes). The results are the average and standard deviation over two replicate wells.

Studies with pharmacological inhibitors of endocytosis

To investigate the role of different endocytic pathways and cellular structures in nanoparticle uptake in the cell barriers and confluent cells, cells were treated with pharmacological inhibitors and nanoparticle uptake in cells exposed to the different drugs was compared to that in untreated cells. Each inhibitor concentration was optimized in order to limit cell death during the experimental period and to maximize the drug efficacy. Briefly, 3000 cells cm^{-2} were seeded in a 24-well plate coated with rat-tail collagen type I and cultured for 7 days as described above in order to form cell barriers. Additionally, to study uptake mechanisms in confluent cells, cells were seeded at a density of 25000 cells cm^{-2} and cultured for 1 day. Then, cells were pre-incubated for 10 minutes in serum-free medium supplemented with the different inhibitors at the following concentrations: chlorpromazine hydrochloride (CP) (5 μg ml^{-1}), methyl-β-cyclodextrin (MβCD) (2 mg ml^{-1}), dynasore (Dyn) (30 μg ml^{-1}) (all from Sigma-Aldrich St. Luis, USA), nocodazole (NZ) (5 μM) (Biovision, California, USA), cytochalasin D (CytoD) (0.5 μg ml^{-1}) (Life technologies, NY, USA). Additional drug concentrations were tested for optimization of these protocols (as detailed in Supplementary Information, Figures S17 to S21). After the pre-incubation with the drug, 50 nm red SiO_2 nanoparticles dispersed in human serum (4 mg ml^{-1}) where added to the cells in the presence of the drug. Alternatively, the uptake of fluorescently labelled endocytic markers was used as a control of the efficacy of the drugs. Fluorescently labelled Low Density Lipoprotein (BODIPY LDL, Life technologies, NY, USA) (2 μg ml^{-1} in serum free medium) was used as a marker for clathrin-mediated endocytosis. Uptake of BODIPY lactosylceramide/BSA complex (BODIPY LacCer; Life technologies, NY, USA) (1 μg ml^{-1} in serum free medium) was measured to verify the effect of cholesterol depletion. Samples were collected and prepared for flow cytometry as described above and the fluorescence intensity of at least 20000 cells was measured in triplicate for each time point using a Cytoflex Flow Cytometer (Beckman Coulter, Woerden, the Netherlands) with a 488 nm laser. Normalized uptake data were calculated by dividing the averaged median fluorescence of cells exposed to the nanoparticles or control markers in the presence of the inhibitors with the averaged median fluorescence of control cells exposed for the same time to the same nanoparticles or control markers without inhibitors. From the normalized uptake data, the percentage of reduction of uptake are calculated by subtraction (Uptake reduction % = 100% - normalized uptake %)

Acknowledgements

Inge Zuhorn, Edwin de Jong and Sven C. D. van IJzendoorn (Cell Biology Department, University Medical Center Groningen (UMCG)) are acknowledged for access to TEER measurements and useful discussions on cell barrier formation. Ingrid Molema and Henk

Moorlag (Endothelial Biomedicine & Vascular Drug Targeting, UMCG) are acknowledged for fruitful discussions on endothelial cell models and support in endothelial cell culture. Klaas Sjollema (UMCG Microscopy and Imaging Center, Groningen) is acknowledged for support with confocal fluorescence imaging. This work was funded by the European Research Council (ERC) under the European Union's Horizon 2020 research and innovation programme under grant agreement №637614 (NanoPaths). A.S. kindly acknowledges the University of Groningen for additional funding (Rosalind Franklin Fellowship).

Bibliography

1. Bareford, L. M. & Swaan, P. W. Endocytic mechanisms for targeted drug delivery. *Adv. Drug Deliv. Rev.* **59,** 748–758 (2007).
2. Chithrani, B. D., Ghazani, A. a. & Chan, W. C. W. Determining the size and shape dependence of gold nanoparticle uptake into mammalian cells. *Nano Lett.* **6,** 662–668 (2006).
3. Salvati, A. *et al.* Experimental and theoretical comparison of intracellular import of polymeric nanoparticles and small molecules: Toward models of uptake kinetics. *Nanomedicine Nanotechnology, Biol. Med.* **7,** 818–826 (2011).
4. Sahay, G., Alakhova, D. Y. & Kabanov, A. V. Endocytosis of nanomedicines. *J. Control. Release* **145,** 182–195 (2010).
5. Duncan, R. & Richardson, S. C. W. Endocytosis and intracellular trafficking as gateways for nanomedicine delivery: Opportunities and challenges. *Mol. Pharm.* **9,** 2380–2402 (2012).
6. Rejman, J., Oberle, V., Zuhorn, I. S. & Hoekstra, D. Size-dependent internalization of particles via the pathways of clathrin- and caveolae-mediated endocytosis. *Biochem. J.* **377,** 159–169 (2004).
7. Danhier, F., Feron, O. & Préat, V. To exploit the tumor microenvironment: Passive and active tumor targeting of nanocarriers for anti-cancer drug delivery. *J. Control. Release* **148,** 135–146 (2010).
8. Chauhan, V. P. & Jain, R. K. Strategies for advancing cancer nanomedicine. *Nat. Mater.* **12,** 958–962 (2013).
9. Jain, R. K. Transport of Molecules in the Tumor Interstitium : A Review. *Cancer Res.* **47,** 3039–3051 (1987).
10. Matsumura, Y. & Maeda, H. A new concept for macromolecular therapies in cancer chemotherapy: mechanisms of tumortropic accumulation of proteins and the antitumor agents SMANCS. *Cancer Res.* **6,** 6387–6392 (1986).
11. Tietjen, G. T. & Saltzman, W. M. Nanomedicine gets personal. *Sci. Transl. Med.* **7,** 314fs47 (2015).
12. Miller, M. A. *et al.* Predicting therapeutic nanomedicine efficacy using a companion magnetic resonance imaging nanoparticle. *Sci. Transl. Med.* **7,** 314ra183 (2015).
13. Danhier, F. To exploit the tumor microenvironment: Since the EPR effect fails in the clinic, what is the future of nanomedicine? *J. Control. Release* **244,** 108–121 (2016).
14. Wilhelm, S. *et al.* Analysis of nanoparticle delivery to tumours. *Nat. Rev. Mater.* **1,** 16014 (2016).
15. Torrice, M. Does Nanomedicine Have a Delivery Problem? *ACS Cent. Sci.* **2,** 434–437 (2016).
16. Venditto, V. J. & Szoka, F. C. Cancer Nanomedicines: So Many Papers and So Few Drugs! *Adv Drug Deliv Rev* **65,** 80–88 (2013).
17. Lammers, T. *et al.* Cancer nanomedicine: Is targeting our target? *Nat Rev Mater* **1,** 16069 (2016).
18. Iversen, T. G., Skotland, T. & Sandvig, K. Endocytosis and intracellular transport of nanoparticles: Present knowledge and need for future studies. *Nano Today* **6,** 176–185 (2011).
19. Editorial. Time to deliver. *Nat. Biotechnol.* **32,** 961 (2014).
20. Yameen, B. *et al.* Insight into nanoparticle cellular uptake and intracellular targeting. *J. Control. Release* **190,** 485–499 (2014).
21. Blanco, E., Shen, H. & Ferrari, M. Principles of nanoparticle design for overcoming biological barriers to drug delivery. *Nat. Biotechnol.* **33,** 941–951 (2015).
22. Jain, R. K. Barriers to drug delivery in solid tumors. *Sci. Am.* **271,** 58–65 (1994).
23. Muro, S. Challenges in design and characterization of ligand-targeted drug delivery systems. *J. Control. Release* **164,** 125–137 (2012).

24. Setyawati, M. I., Tay, C. Y., Docter, D., Stauber, R. H. & Leong, D. T. Understanding and exploiting nanoparticles' intimacy with the blood vessel and blood. *Chem. Soc. Rev.* **44,** 8174–8199 (2015).

25. Zhang, Y. & Yang, W.-X. Tight junction between endothelial cells: the interaction between nanoparticles and blood vessels. *Beilstein J. Nanotechnol.* **7,** 675–684 (2016).

26. Dejana, E. Endothelial cell–cell junctions: happy together. *Nat. Rev. Mol. Cell Biol.* **5,** 261–270 (2004).

27. Sandvig, K. & van Deurs, B. Delivery into cells: lessons learned from plant and bacterial toxins. *Gene Ther.* **12,** 865–872 (2005).

28. Lin, I. C., Liang, M., Liu, T. Y., Monteiro, M. J. & Toth, I. Cellular transport pathways of polymer coated gold nanoparticles. *Nanomedicine Nanotechnology, Biol. Med.* **8,** 8–11 (2012).

29. Li, C. H. *et al.* Gold nanoparticles increase endothelial paracellular permeability by altering components of endothelial tight junctions, and increase blood-brain barrier permeability in mice. *Toxicol. Sci.* **148,** 192–203 (2015).

30. Ghaffarian, R., Bhowmick, T. & Muro, S. Transport of nanocarriers across gastrointestinal epithelial cells by a new transcellular route induced by targeting ICAM-1. *J. Control. Release* **163,** 25–33 (2012).

31. Ulbrich, K., Knobloch, T. & Kreuter, J. Targeting the insulin receptor: Nanoparticles for drug delivery across the blood-brain barrier (BBB). *J. Drug Target.* **19,** 125–132 (2011).

32. Pardridge, W. M. Drug Transport across the Blood–Brain Barrier. *J. Cereb. Blood Flow Metab.* **32,** 1959–1972 (2012).

33. Kreuter, J. Nanoparticulate systems for brain delivery of drugs. *Adv. Drug Deliv. Rev.* **47,** 65–81 (2001).

34. Georgieva, J. V., Hoekstra, D. & Zuhorn, I. S. Smuggling drugs into the brain: An overview of ligands targeting transcytosis for drug delivery across the blood–brain barrier. *Pharmaceutics* **6,** 557–583 (2014).

35. Georgieva, J. V. *et al.* Surface Characteristics of Nanoparticles Determine Their Intracellular Fate in and Processing by Human Blood–Brain Barrier Endothelial Cells In Vitro. *Mol. Ther.* **19,** 318–325 (2011).

36. dos Santos, T., Varela, J., Lynch, I., Salvati, A. & Dawson, K. a. Effects of transport inhibitors on the cellular uptake of carboxylated polystyrene nanoparticles in different cell lines. *PLoS One* **6,** e24438 (2011).

37. Vercauteren, D. *et al.* The Use of Inhibitors to Study Endocytic Pathways of Gene Carriers : Optimization and Pitfalls. *Mol. Ther.* **18,** 561–569 (2010).

38. Harush-Frenkel, O., Rozentur, E., Benita, S. & Altschuler, Y. Surface charge of nanoparticles determines their endocytic and transcytotic pathway in polarized MDCK cells. *Biomacromolecules* **9,** 435–443 (2008).

39. Wang, C., de Jong, E., Sjollema, K. A. & Zuhorn, I. S. Entry of PIP3-containing polyplexes into MDCK epithelial cells by local apical-basal polarity reversal. *Sci. Rep.* **6,** 21436 (2016).

40. Ye, D. *et al.* Low uptake of silica nanoparticles in Caco-2 intestinal epithelial barriers. *Beilstein J. Nanotechnol.* **8,** 1396–1406 (2017).

41. Bramini, M. *et al.* Imaging approach to mechanistic study of nanoparticle interactions with the blood-brain barrier. *ACS Nano* **8,** 4304–4312 (2014).

42. Ilina, P. *et al.* Effect of differentiation on endocytic profiles of endothelial and epithelial cell culture models. *Exp. Cell Res.* **332,** 89–101 (2015).

43. Bimbo, L. M. *et al.* Drug permeation across intestinal epithelial cells using porous silicon nanoparticles. *Biomaterials* **32,** 2625–2633 (2011).

44. Yang, Y.-X. *et al.* Evaluation of the toxicity of food additive silica nanoparticles on gastrointestinal cells. *J. Appl. Toxicol.* **34,** 424–435 (2014).

45. He, B. *et al.* The transport mechanisms of polymer nanoparticles in Caco-2 epithelial cells. *Biomaterials* **34,** 6082–6098 (2013).

46. Walczak, A. P. *et al.* Translocation of differently sized and charged polystyrene nanoparticles in in vitro intestinal cell models of increasing complexity. *Nanotoxicology* **9,** 453–561 (2015).

47. Park, H.-J. *et al.* Human Umbilical Vein Endothelial Cells and Human Dermal Microvascular Endothelial Cells Offer New Insights Into the Relationship Between Lipid Metabolism and Angiogenesis. *Stem Cell Rev.* **2,** 93–102 (2006).

48. Gunduz, N., Ceylan, H., Guler, M. O. & Tekinay, A. B. Intracellular Accumulation of Gold Nanoparticles Leads to Inhibition of Macropinocytosis to Reduce the Endoplasmic Reticulum Stress. *Sci. Rep.* **7,** 1–10 (2017).

49. Key, J. *et al.* Soft Discoidal Polymeric Nanoconstructs Resist Macrophage Uptake and Enhance Vascular Targeting in Tumors. *ACS Nano* **9,** 11628–11641 (2015).

50. Ho, Y. T. *et al.* A Facile Method to Probe the Vascular Permeability of Nanoparticles in Nanomedicine Applications. *Sci. Rep.* **7,** 1–13 (2017).

51. Davda, J. & Labhasetwar, V. Characterization of nanoparticle uptake by endothelial cells. *Int. J. Pharm.* **233,** 51–59 (2002).

52. Liu, Y. *et al.* Nanoparticle size-specific actin rearrangement and barrier dysfunction of endothelial cells. *Nanotoxicology* **11,** 846–856 (2017).

53. dos Santos, T., Varela, J., Lynch, I., Salvati, A. & Dawson, K. A. Quantitative Assessment of the Comparative Nanoparticle-Uptake Efficiency of a Range of Cell Lines. *Small* **7,** 3341–3349 (2011).

54. Samuel, S. P. *et al.* Multifactorial determinants that govern nanoparticle uptake by human endothelial cells under flow. *Int. J. Nanomedicine* **7,** 2943–2956 (2012).

55. Klingberg, H., Loft, S., Oddershede, L. B. & Møller, P. The influence of flow, shear stress and adhesion molecule targeting on gold nanoparticle uptake in human endothelial cells. *Nanoscale* **7,** 11409–11419 (2015).

56. Blechinger, J. *et al.* Uptake kinetics and nanotoxicity of silica nanoparticles are cell type dependent. *Small* **9,** 3970–3980 (2013).

57. Minami, H. *et al.* Generation of brain microvascular endothelial-like cells from human induced pluripotent stem cells by co-culture with C6 glioma cells. *PLoS One* **10,** 1–13 (2015).

58. Patkar, C., Giaya, K. & Libraty, D. H. Dengue virus type 2 modulates endothelial barrier function through CD73. *Am. J. Trop. Med. Hyg.* **88,** 89–94 (2013).

59. Dewi, B. E., Takasaki, T. & Kurane, I. In vitro assessment of human endothelial cell permeability: Effects of inflammatory cytokines and dengue virus infection. *J. Virol. Methods* **121,** 171–180 (2004).

60. Han, J. *et al.* Involvement of histamine and rhoa/rock in penicillin immediate hypersensitivity reactions. *Sci. Rep.* **6,** 1–14 (2016).

61. Itagaki, K. *et al.* Sphingosine 1-Phosphate Has Dual Functions in the Regulation of Endothelial Cell Permeability and Ca 2ε Metabolism. *Pharmacology* **323,** 186–191 (2007).

62. Krohne, T. U., Holz, F. G. & Kopitz, J. Apical-to-Basolateral Transcytosis of Photoreceptor Outer Segments Induced by Lipid Peroxidation Products in Human Retinal Pigment Epithelial Cells. *Investig. Opthalmology Vis. Sci.* **51,** 553 (2010).

63. Ragnaill, M. N. *et al.* Internal benchmarking of a human blood-brain barrier cell model for screening of nanoparticle uptake and transcytosis. *Eur. J. Pharm. Biopharm.* **77,** 360–367 (2011).

64. Hadjidemetriou, M. & Kostarelos, K. Nanomedicine: Evolution of the nanoparticle corona. *Nat. Nanotechnol.* **12,** 288–290 (2017).

65. Nel, A. E. *et al.* Understanding biophysicochemical interactions at the nano-bio interface. *Nat. Mater.* **8,** 543–557 (2009).

66. Lara, S. *et al.* Identification of Receptor Binding to the Biomolecular Corona of Nanoparticles. *ACS Nano* **11,** 1884–1893 (2017).

67. Salvati, A. *et al.* Transferrin-functionalized nanoparticles lose their targeting capabilities when a biomolecule corona adsorbs on the surface. *Nat. Nanotechnol.* **8,** 137–43 (2013).

68. Kim, J. A., Åberg, C., Salvati, A. & Dawson, K. A. Role of cell cycle on the cellular uptake and dilution of nanoparticles in a cell population. *Nat. Nanotechnol.* **7,** 62–68 (2011).

69. Hunt, M. A., Currie, M. J., Robinson, B. A. & Dachs, G. U. Optimizing transfection of primary human umbilical vein endothelial cells using commercially available chemical transfection reagents. *J. Biomol. Tech.* **21,** 66–72 (2010).

70. Dennstedt, E. & Bryan, B. in *Therapeutic Oligonucleotides: Methods and Protocols* (ed. Goodchild, J.) 215–222 (Humana Press, 2011). doi:10.1007/978-1-61779-188-8_14

71. Wang, L.-H., Rothberg, K. G. & Anderson, R. G. W. Mis-assembly of clathrin lattices on endosomes reveals a regulatory switch for coated pit formation. *J. Cell Biol.* **123,** 1107–1117 (1993).

72. Macia, E. *et al.* Dynasore, a Cell-Permeable Inhibitor of Dynamin. *Dev. Cell* **10,** 839–850 (2006).

73. Hubatsch, I., Ragnarsson, E. G. E. & Artursson, P. Determination of drug permeability and prediction of drug absorption in Caco-2 monolayers. *Nat. Protoc.* **2,** 2111–2119 (2007).

74. Foerg, C., Ziegler, U., Fernandez-Carneado, J., Giralt, E. & Merkle, H. P. Differentiation restricted endocytosis of cell penetrating peptides in MDCK cells corresponds with activities of Rho-GTPases. *Pharm. Res.* **24,** 628–642 (2007).

75. von Bonsdorff, C. H., Fuller, S. D. & Simons, K. Apical and basolateral endocytosis in Madin-Darby canine kidney (MDCK) cells grown on nitrocellulose filters. *EMBO J.* **4,** 2781–2792 (1985).

76. Naim, H. Y., Dodds, D. T., Brewer, C. B. & Roth, M. G. Apical and basolateral coated pits of MDCK cells differ in their rates of maturation into coated vesicles, but not in the ability to distinguish between mutant hemagglutinin proteins with different internalization signals. *J. Cell Biol.* **129,** 1241–1250 (1995).

77. Bayless, K. J., Kwak, H.-I. & Su, S.-C. Investigating endothelial invasion and sprouting behavior in three-dimensional collagen matrices. *Nat. Protoc.* **4,** 1888 (2009).

78. Morigi, M. *et al.* Fluid shear stress modulates surface expression of adhesion molecules by endothelial cells. *Blood* **85,** 1696–1703 (1995).

79. Ucciferri, N. *et al.* In vitro toxicological screening of nanoparticles on primary human endothelial cells and the role of flow in modulating cell response. *Nanotoxicology* **8,** 697–708 (2014).

80. Bhowmick, T., Berk, E., Cui, X., Muzykantov, V. R. & Muro, S. Effect of flow on endothelial endocytosis of nanocarriers targeted to ICAM-1. *J. Control. Release* **157,** 485–492 (2012).

81. Hadjidemetriou, M. *et al.* In Vivo Biomolecule Corona around Blood-Circulating, Clinically Used and Antibody-Targeted Lipid Bilayer Nanoscale Vesicles. *ACS Nano* **9,** 8142–8156 (2015).

82. Moore, T. L. *et al.* Cellular Shuttles: Monocytes/Macrophages Exhibit Transendothelial Transport of Nanoparticles under Physiological Flow. *ACS Appl. Mater. Interfaces* **9,** 18501–18511 (2017).

83. Fede, C. *et al.* Evaluation of gold nanoparticles toxicity towards human endothelial cells under static and flow conditions. *Microvasc. Res.* **97,** 147–155 (2015).

84. Gerhardt, C. F. & H. Blood vessels on a chip. *Nature* **488,** 465–466 (2012).

85. Zheng, Y. *et al.* In vitro microvessels for the study of angiogenesis and thrombosis. *Proc. Natl. Acad. Sci.* **109,** 9342–9347 (2012).

Supplementary Information

Gene	Forward (left)	Reverse (right)
CAV1	ACAGCCCAGGGAAACCTC	GATGGGAACGGTGTAGAGATG
CDC42	CATCGGAATATGTACCGACTGTT	TGCAGTATCAAAAAGTCCAAGAGTA
CLTC	TGAGAAAAGAAGAAGAACAAGCTACA	ACACTGGGTCCTGCTGTCA
RHOA	GGAGCTAGCCAAGATGAAGC	GCCAATCCTGTTTGCCATA
ARF6	TGAACACAAAGTTGCTAGATGCT	TGCTGTGTTTCCCCCATC
TFRC	TGAAGAGAAAGTTGTCGGAGAAA	CAGCCTCACGAGGGACATA
DNM2	CATCAACACGAACCATGAGG	CTTGTTCAGCTGCGTGCTC
FLOT1	ATTCTAACTCGCCTGCCAGA	GCATCTGTGAGGGCTGAAG
LDLR	GTGACAATGTCTCACCAAGCTC	CACGCTACTGGGCTTCTTCT
ARHGAP26	CAGGCACGGTCTTCGATAA	GCCAGTCTTTCCGTTCAGAG
RAC1	CTGATCAGTTACACAACCAATGC	CATTGGCAGAATAATTGTCAAAGA
ANKFY1	AAACTAGCAAATCGGTTTCAGC	GAGACATAACACCCTTCTCACATC
EPN1	GAGAGCAAGAGGGAGACTGG	AAGACGTCAGCAAGGTCCAT

Table S1. Primers used in this study for RT-qPCR. RT-qPCR was performed as described in the Experimental Section to determine the expression levels of some cell receptors (LDL and transferrin receptor), and a series of targets involved in different endocytic pathways.

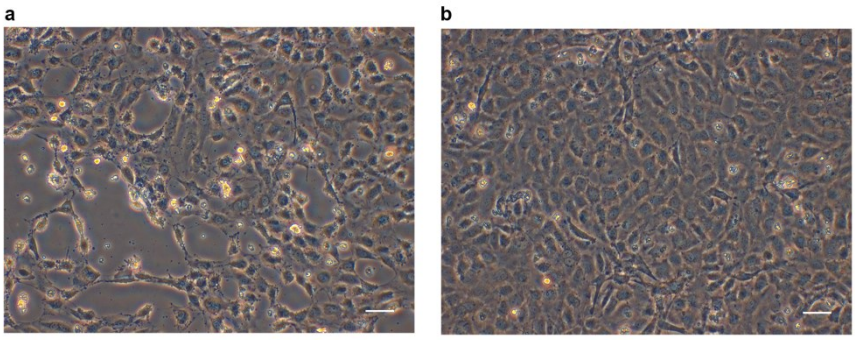

Figure S1. Effect of surface coating on cell growth. Representative light microscopy images of HUVEC plated at a concentration of 10000 cells cm^{-2} on 24 well plates uncoated (a) or coated with rat tail collagen Type-I (b). Scale bar 50 µm. The presence of a collagen coating clearly improved cell adherence and cell growth.

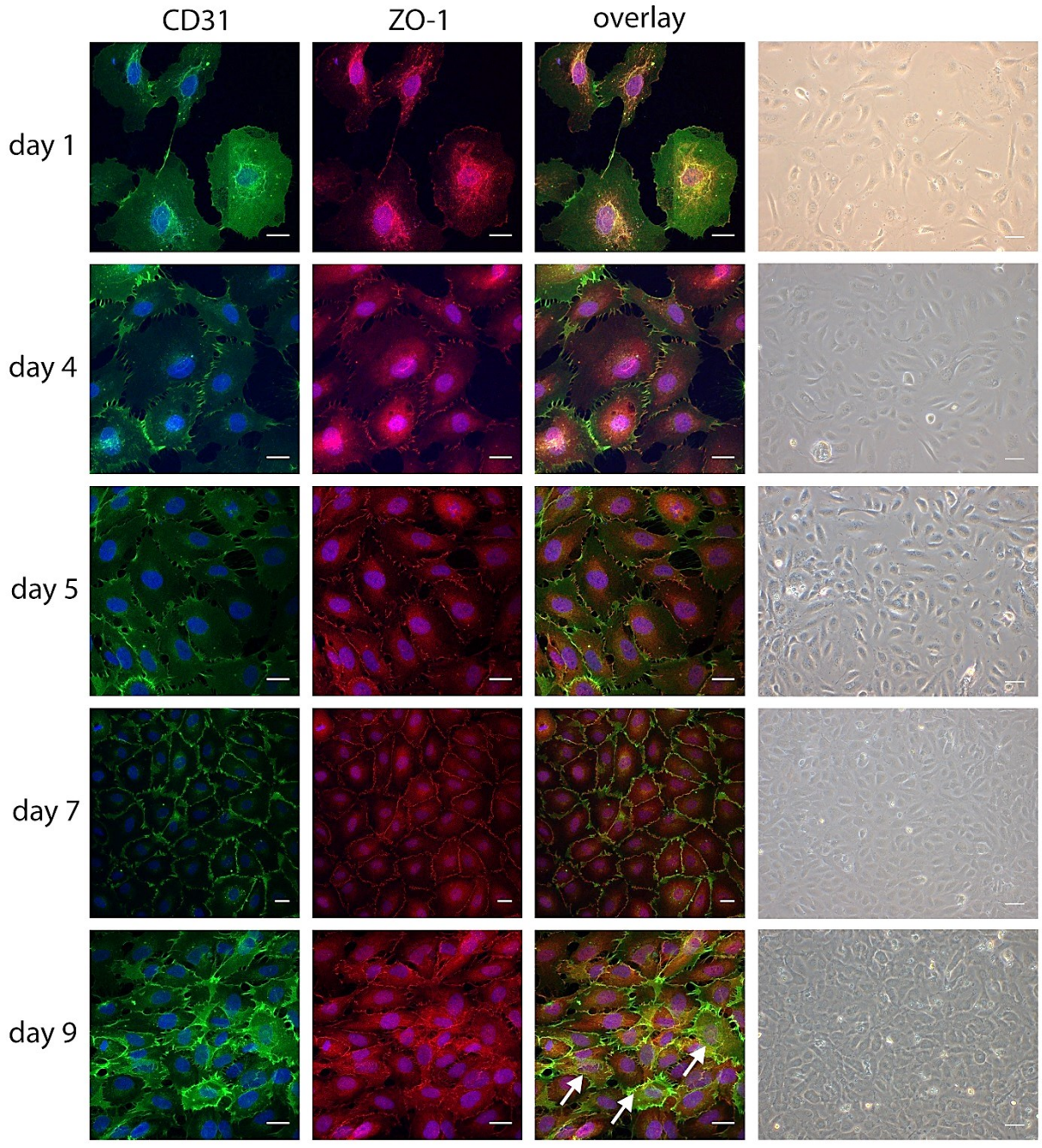

Figure S2. HUVEC barrier formation from low cell density cultures. 3000 cells cm-2 HUVEC were plated on collagen coated glass coverslips and their growth was monitored for different days after seeding. Left: confocal images of HUVEC cells stained with anti-ZO-1 (red) or anti-CD31 (green) antibodies. Blue: DAPI stained nuclei (scale bar: 20 µm). Right: light microscopy images of the same cultures (scale bar: 50 µm). Tight junction staining showed barrier formation roughly 7 days after cell seeding, then cells started to strongly overlap in multiple layers (as indicated by the white arrows) and areas with holes in the cell monolayer were observed, as a consequence of cell death.

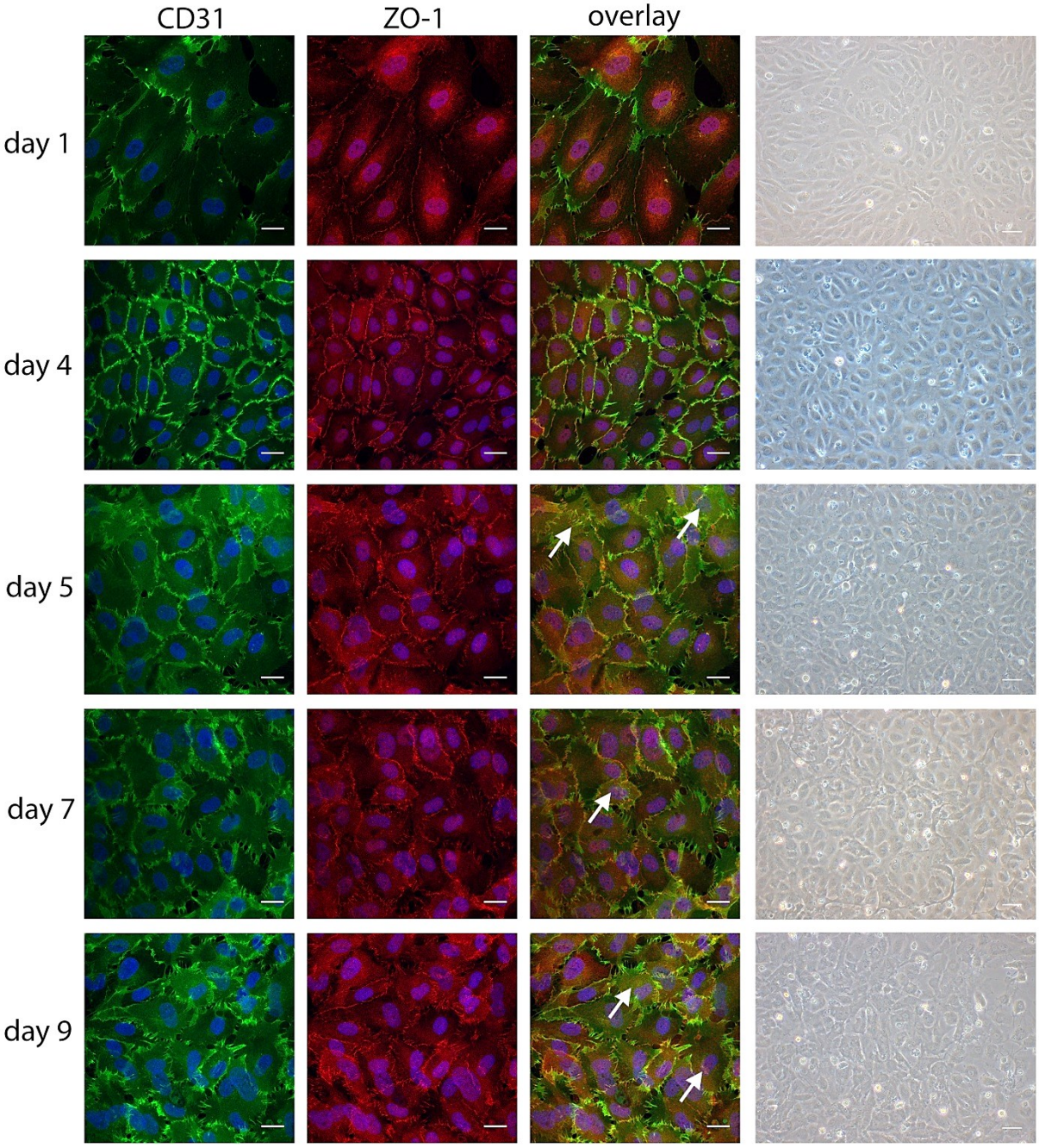

Figure S3. HUVEC barrier formation from high cell density cultures. 50000 cells cm-2 HUVEC were plated on collagen coated glass coverslips and their growth was monitored for different days after seeding. Left: confocal images of HUVEC cells stained with anti-ZO-1 (red) or anti-CD31 (green) antibodies. Blue: DAPI stained nuclei (scale bar: 20 µm). Right: light microscopy images of the same cultures (scale bar: 50 µm). Tight junction staining showed barrier formation roughly 4 days after cell seeding, then cells started to overlap in multiple layers (as indicated by the white arrows) and areas with holes in the cell monolayer were observed, as a consequence of cell death.

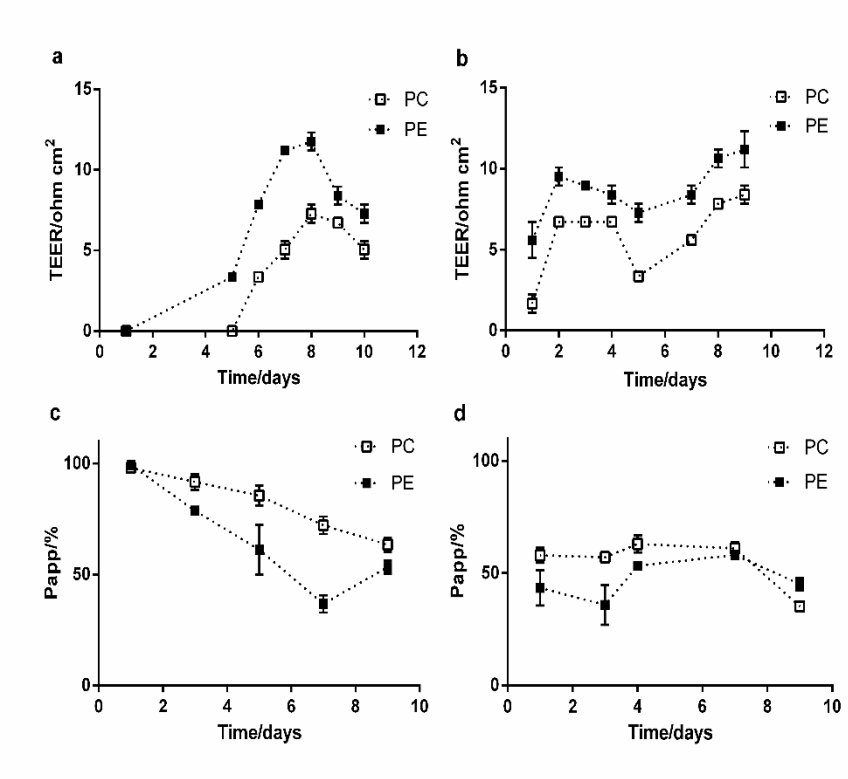

Figure S4. Optimization of HUVEC barrier formation. HUVEC were seeded at two concentrations (3000 cells cm-2, (a) and (c) or 50000 cells cm-2, (b) and (d)) on Transwell® inserts made of polyester (PE) or polycarbonate (PC) and barrier formation was monitored for several days after seeding. a, b: Trans Epithelial Electrical Resistance (TEER) at different times after seeding. Results are the average TEER value and standard deviation obtained from two different inserts which were measured over time for the entire experimental period. c, d: Apparent permeability (Papp) of FITC-Dextran (4 kDa, 200 µg ml-1). The fluorescence intensity of FITC-Dextran in the basal chamber was used to calculate the apparent permeability as described in the Experimental Section. Results are the average value and standard deviation of 2 different inserts, normalized by the results obtained on Transwells without cells. Overall the results show that PE is a better substrate than PC for cell growth and barrier formation, and that seeding cells at lower density and waiting longer allowed HUVEC to develop into a cell barrier with high electrical resistance and a low permeability in about 7 days after seeding.

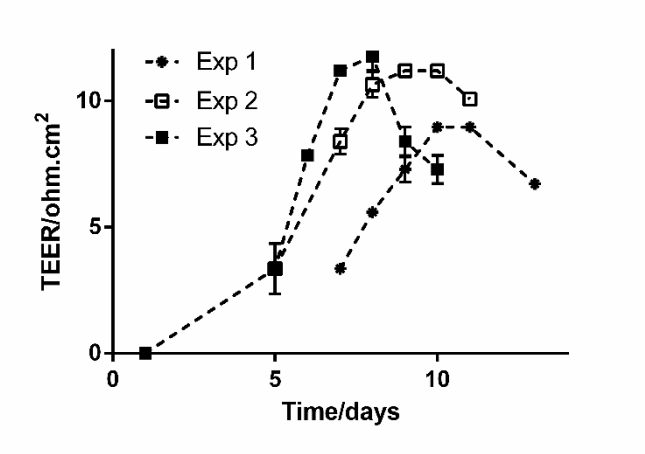

Figure S5. Trans Epithelial Electrical Resistance (TEER) of HUVEC layers formed on polyester (PE) filters. 3000 cells cm-2. HUVEC were seeded on polyester Transwells as described in the Experimental Section and their TEER measured at the indicated times after seeding. Results are the average TEER value and standard deviation obtained from two different inserts which were measured over time for the entire experimental period. Even though in independent experiments the absolute TEER values were rather variable, the trend was consistent and in all cases, it showed a progressive increase of TEER at increasing days after seeding, with a peak reached 7-8 days after seeding, sign of barrier formation, followed by a progressive decrease as a consequence of cell death.

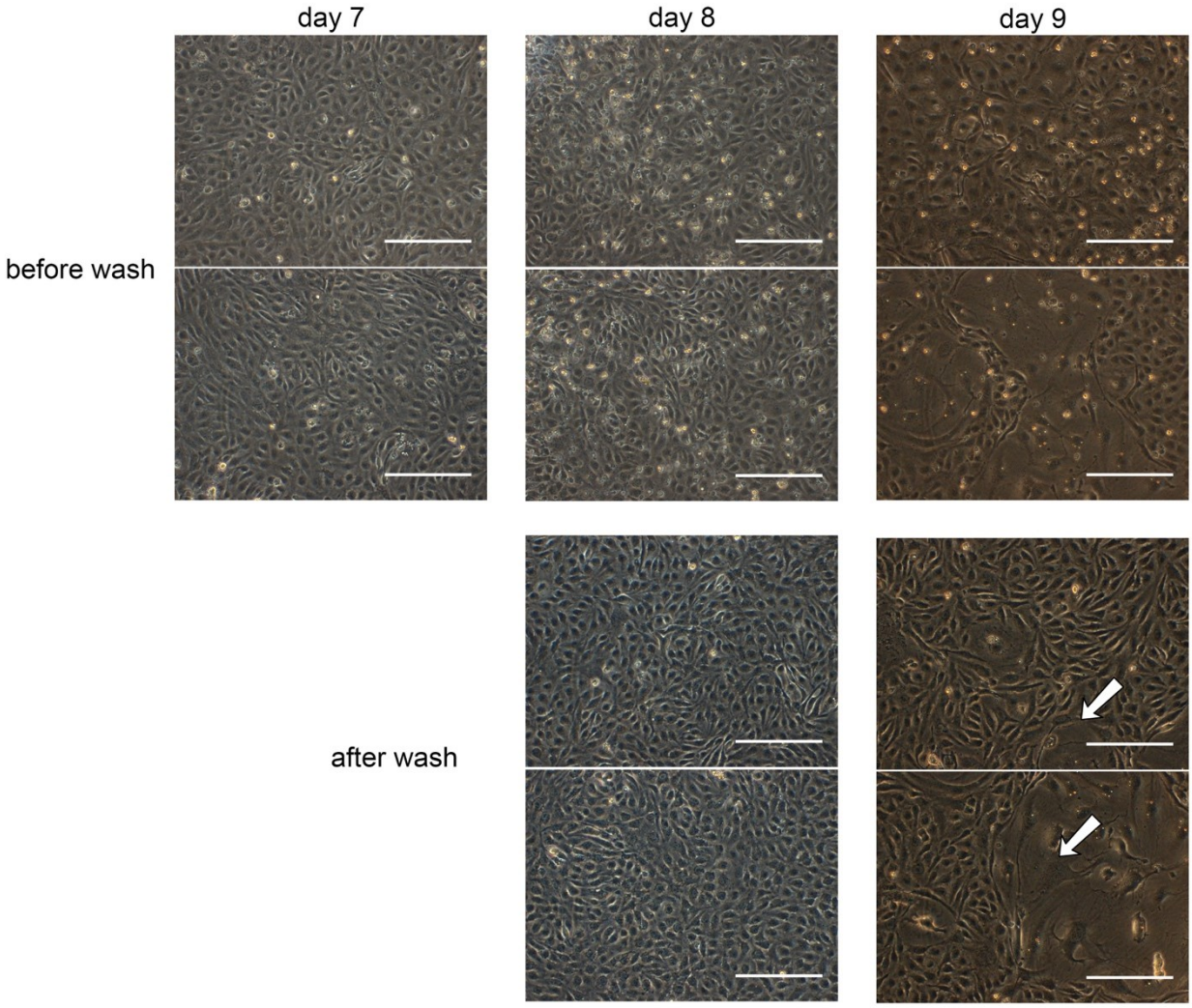

Figure S6. Integrity of HUVEC barriers formed from low cell density cultures. Representative light microscopy images before and after washing of HUVEC cell barriers formed from low cell density cultures, plated at a concentration of 3000 cells cm-2 on 24 well plates and cultured for the indicated times (scale bar: 200 µm). Roughly 9 days after seeding, before washing the wells, many floating (dead) cells were clearly visible. Consecutively, after washing the wells, holes in the cell monolayer (as indicated by the white arrows) were visible. This overall indicated that in these conditions, roughly 9 days after cell seeding, barrier integrity was lost.

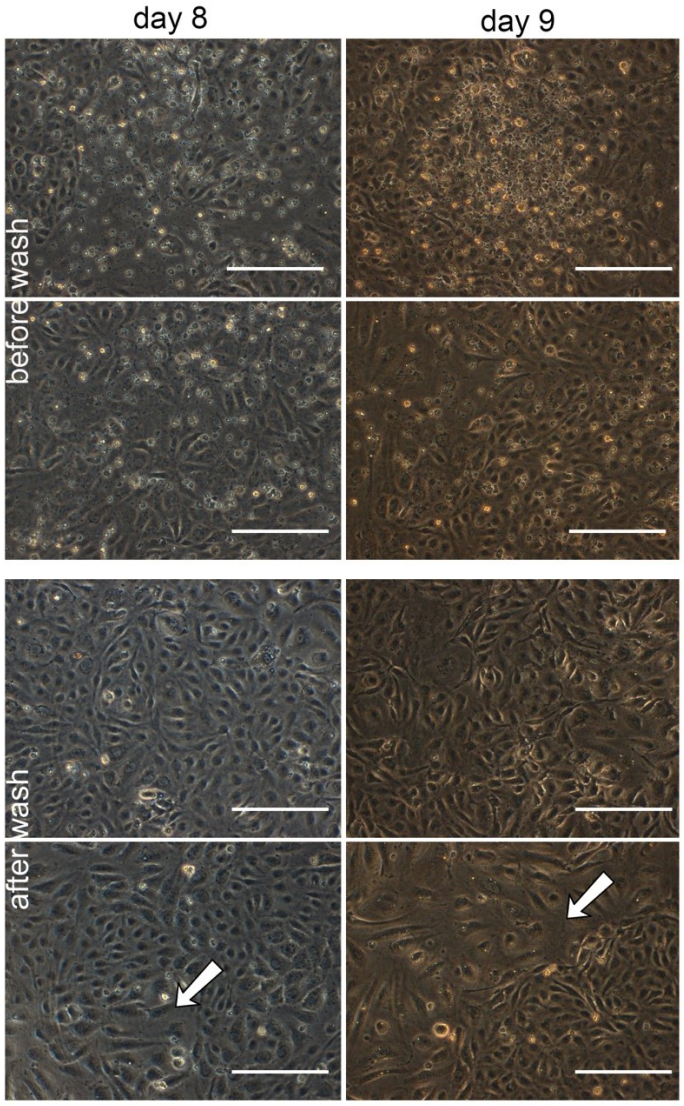

Figure S7. Integrity of HUVEC barriers formed from high cell density cultures. Representative light microscopy images before and after washing of HUVEC cell barriers formed from high cell density cultures, plated at a concentration of 50000 cells cm-2 on 24 well plates and cultured for the indicated times (scale bar: 200 µm). Roughly 8 days after seeding, before washing the wells, many floating (dead) cells were clearly visible. Consecutively, after washing the wells, holes in the cell monolayer (as indicated by the white arrows) were visible. This overall indicated that in these conditions, roughly 8 days after cell seeding, barrier integrity was lost.

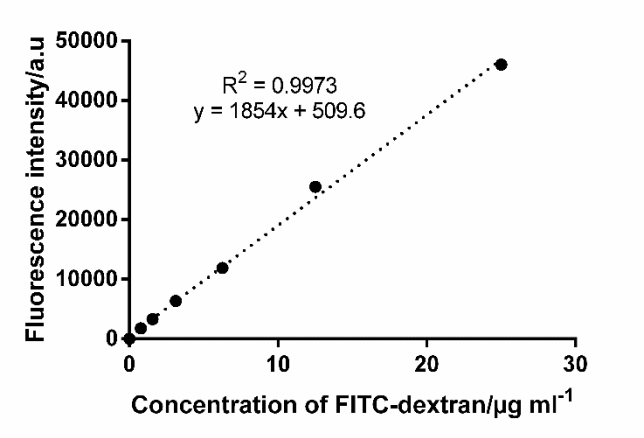

Figure S8. Calibration curve for FITC-Dextran fluorescence. The fluorescence intensity of samples at increasing concentrations of 4 kDa FITC-Dextran was measured using a spectrofluorometer. Linear regression was used to obtain the relation between FITC-dextran concentration and fluorescence, from which the apparent permeability Papp was determined as described in the Experimental Section. A different calibration curve was made for each experiment (R2 values ≥ 0.995 in all cases).

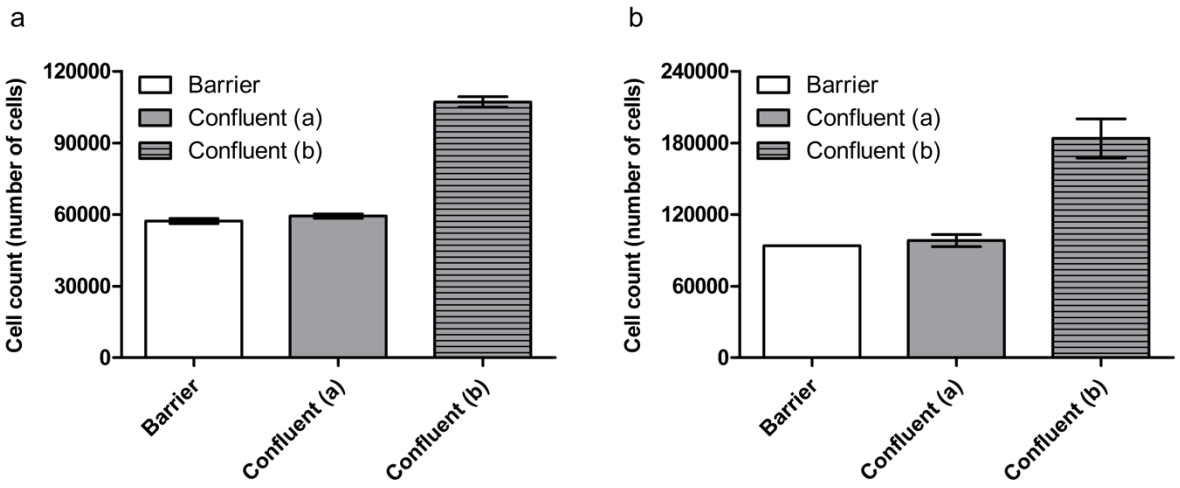

Figure S9. Number of cells in HUVEC barriers and confluent cell cultures. HUVEC barriers and confluent cultures were prepared by seeding 3000 cells cm-2 (barrier) or 25000 cells cm-2 (confluent (a)), and cell numbers were counted 7 days (barrier) or 1 day (confluent) after seeding. Additionally, 50000 cells cm-2 (confluent (b)) were also seeded and cell numbers counted 1 day after seeding, as ulterior control. Cell numbers were counted using a hemocytometer (a) or by flow cytometry (b) as described in the Experimental Section. The results are the average and standard deviation of two replicate wells. The results confirmed that the optimized cell barriers and confluent cell cultures (confluent (a)) had comparable cell numbers. When the double of cells was seeded (confluent (b)), a double number of cells was counted 1 day after seeding, further confirming accuracy in cell seeding and of the two methods used to count cell numbers.

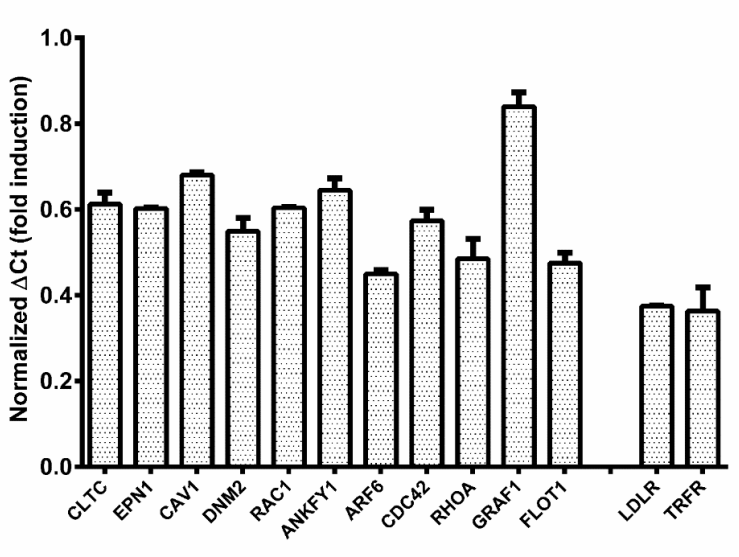

Figure S10. Expression levels of genes coding for endocytic proteins in HUVEC barriers in comparison to confluent cell cultures. HUVEC were seeded at a density of 3000 cells cm-2 and cultured for seven days (barriers) or 25000 cells cm-2 and cultured for one day (confluent cells). RT-qPCR was performed as described in the Experimental Section to determine the expression levels of genes coding for some cell receptors (LDL and transferrin receptors), and for a series of targets involved in clathrin mediated endocytosis (CME), caveolae-mediated endocytosis, macropinocytosis, and other clathrin and caveolae independent mechanisms (see also Supplementary Table S1 for details). Results are the average and standard deviation over 4 replicate wells of the fold-change in gene expression levels in HUVEC barriers compared to confluent cells. The results indicated that the gene expression of the selected endocytic targets in the cell barriers was lower than in confluent cells.

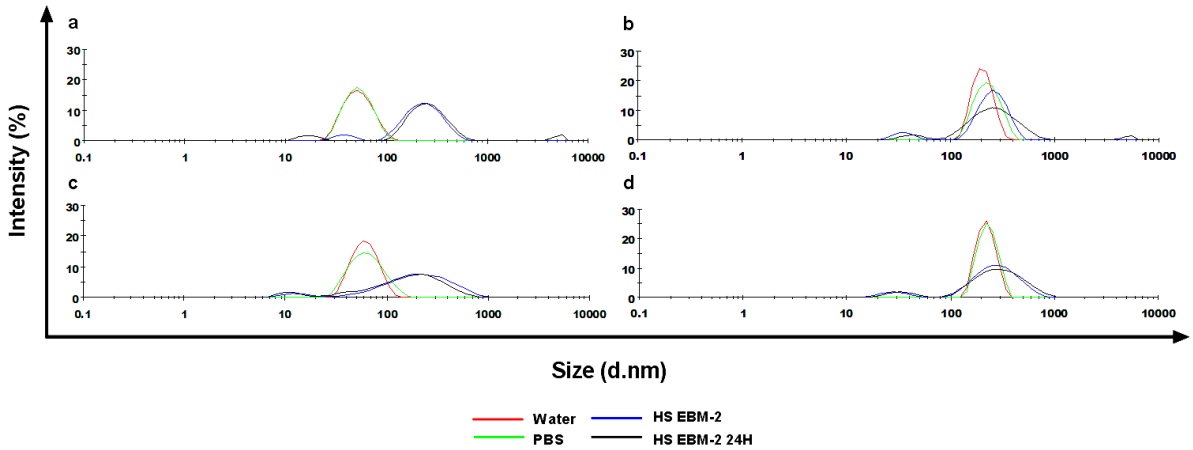

Figure S11. Size distribution by intensity (diameter, d, nm) of 50 nm red SiO2 (a), 200 nm red SiO2 (b), 40 nm red PS-COOH (c) and 200 nm orange PS-COOH (d) as obtained by dynamic light scattering (DLS). Silica nanoparticles (100 µg ml-1) were dispersed in water, PBS, and EBM-2 supplemented with 4 mg ml-1 of human serum (HS EBM-2). For the 40 nm PS-COOH nanoparticles instead (c), in order to determine the size distribution at a nanoparticle to protein ratio closer to that used for cell experiments, 25 µg ml-1 nanoparticles were dispersed in EBM-2 supplemented with 50 mg ml-1 human serum. For the same reasons, the 200 nm PS-COOH nanoparticles (d) were dispersed to a final concentration of 36 µg ml-1 in EBM-2 supplemented with 48 mg ml-1 human serum. Size distributions in HS EBM-2 were measured immediately, or after 24h of incubation of the dispersions at 37 ˚C, 5% CO2 (HS EBM-2 24h). The results showed that all dispersions remained stable for up to 24 hours in the conditions used for cell experiments.

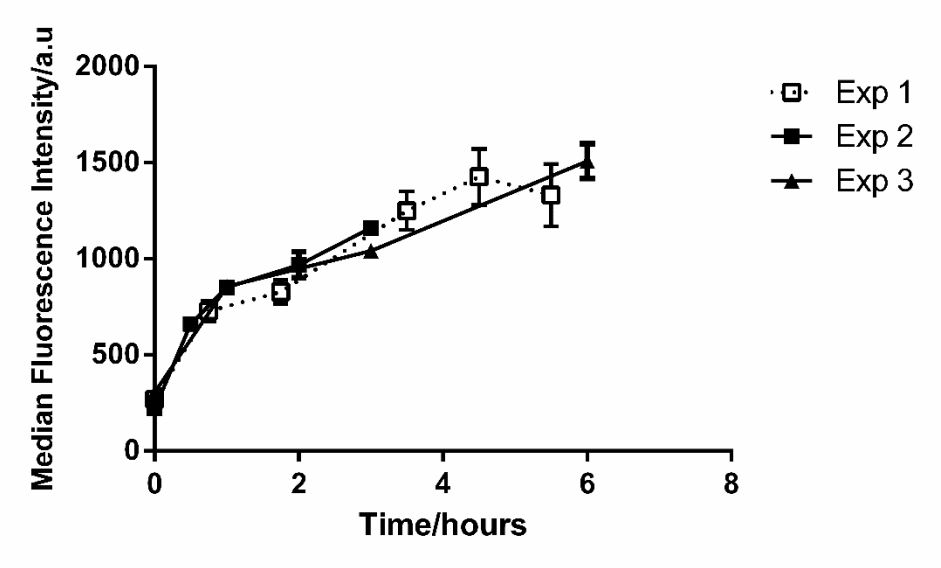

Figure S12. Reproducibility of nanoparticle uptake levels in HUVEC barriers in independent experiments. Median cell fluorescence intensity as obtained by flow cytometry of HUVEC barriers (seven days after seeding 3000 cells cm-2) prepared in independent experiments (Exp 1-3) and exposed for increasing times to 100 µg ml-1 50 nm SiO_2 nanoparticles dispersed in EBM-2 medium supplemented with 4 mg ml-1 human serum. (Exp 1 is from Figure 4f and Exp 2 is from Figure 4l, while Exp 3 is an equivalent independent replica). In the three independent experiments, barriers were formed following the optimized protocols and were exposed to independent nanoparticle dispersions, prepared as described in the Experimental Section, using nanoparticles and human serum from the same batches. Results are the average and standard deviation over three replicates of the median cell fluorescence intensities. Overall the results show that when the same nanoparticle stock and human serum were used to prepare in independent experiments the nanoparticle dispersions, a very good reproducibility in nanoparticle uptake in the cell barriers was obtained. This indicated very good reproducibility of the barrier model, as also of the nanoparticle dispersions and all procedures for exposure to cells and measurement.

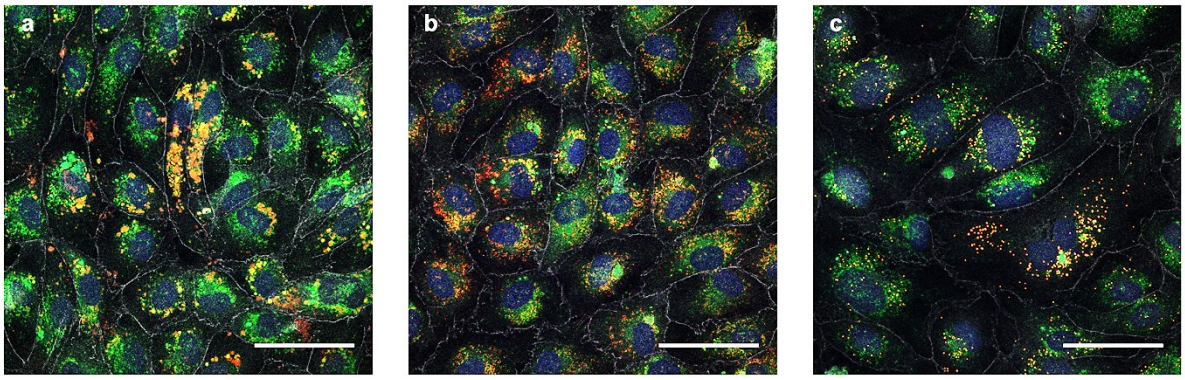

Figure S13. Uptake and intracellular distribution of different nanoparticles in HUVEC barriers. HUVEC barriers (seven days after seeding 3000 cells cm-2) were exposed for 24 hours to 200 µg ml-1 200 nm SiO2 (a), 2 µg ml-1 40 nm PS-COOH (b) or 3 µg ml-1 200 nm PS-COOH (c) nanoparticles in EBM-2 medium supplemented with 4 mg ml-1 human serum. Red: nanoparticles, Green: LAMP-1, Grey: ZO-1, Blue: DAPI. Scale bar: 50 µm.

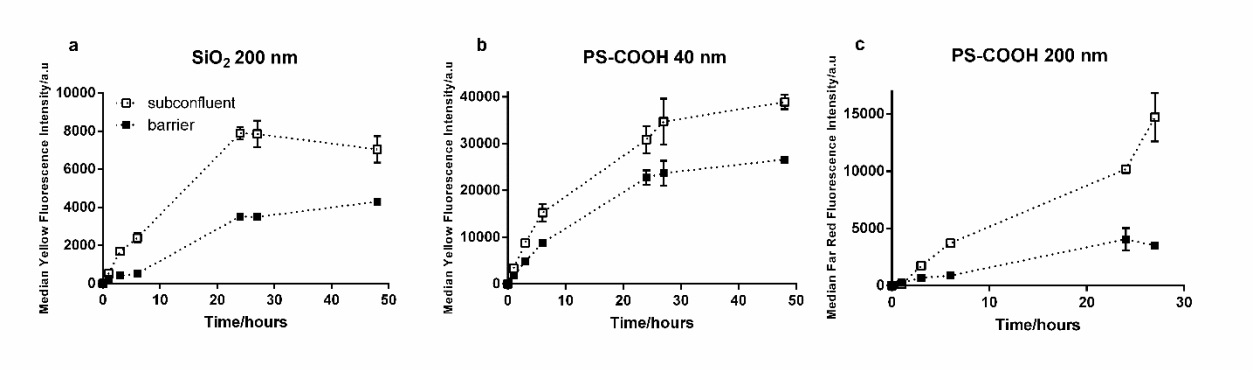

Figure S14. Nanoparticle uptake levels in HUVEC barriers and subconfluent cultures. Median cell fluorescence intensity as obtained by flow cytometry of HUVEC exposed to different nanoparticles. HUVEC were grown for three (subconfluent) or seven (barrier) days after seeding (3000 cells cm-2) and exposed to 200 nm SiO2 (200 µg ml-1, a), 40 nm PS-COOH (2 µg ml-1, b) or 200 nm PS-COOH (3 µg ml-1, c) in EBM-2 medium supplemented with 4 mg ml-1 human serum for the indicated times. Results represent the average median and standard deviation of three replicates (for the 200 nm PS-COOH nanoparticles the far red fluorescence is plotted because the yellow fluorescence in subconfluent cells was out of scale due to the extremely high fluorescence intensity of these nanoparticles and high uptake levels).

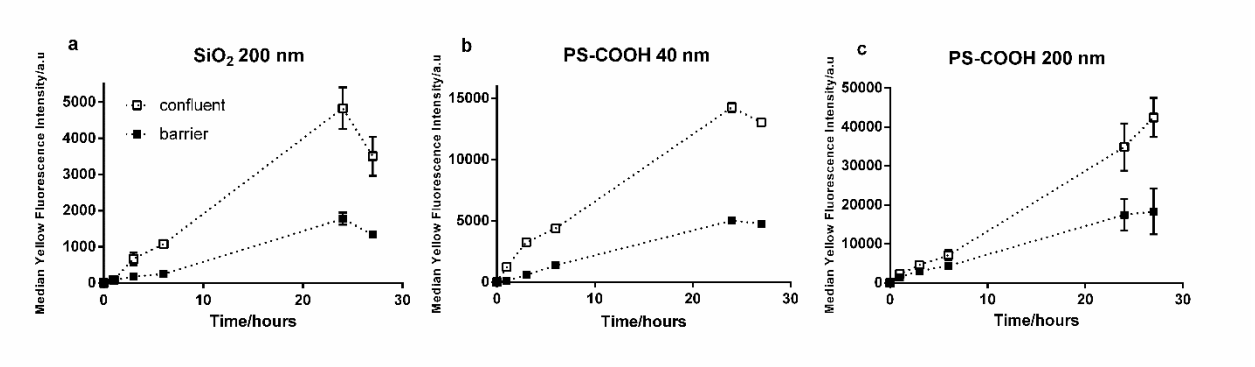

Figure S15. Nanoparticle uptake levels in HUVEC barriers and confluent cultures. Median cell fluorescence intensity as obtained by flow cytometry of HUVEC exposed to different nanoparticles. Confluent HUVEC (one day after seeding 25000 cells cm-2) and HUVEC barriers (seven days after seeding 3000 cells cm-2) were exposed to 200 nm SiO2 (200 µg ml-1, a), 40 nm PS-COOH (2 µg ml-1, b) or 200 nm PS-COOH (3 µg ml-1, c) in EBM-2 medium supplemented with 4 mg ml-1 human serum for the indicated times. Results represent the average median and standard deviation of three replicates.

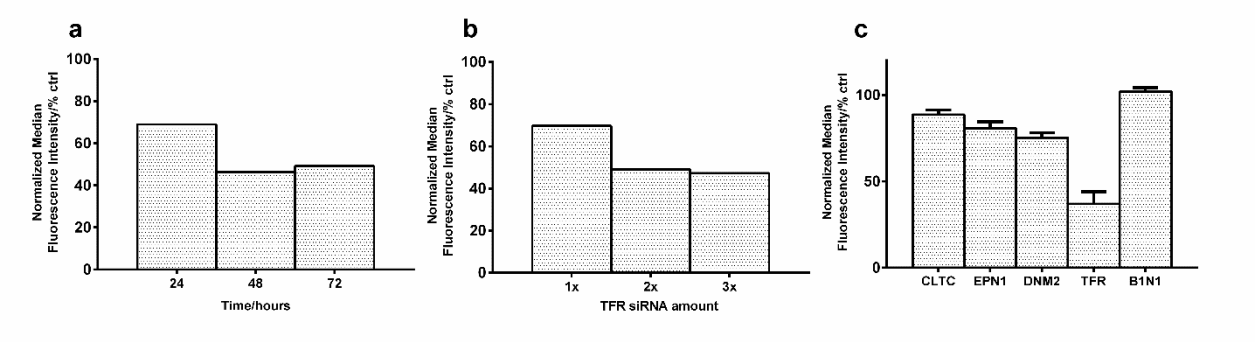

Figure S16. Efficacy of silencing in HUVEC. Uptake of transferrin in HUVEC transfected with siRNA to block the expression of the transferrin receptor (TFRC) and of other targets involved in clathrin mediated endocytosis (CME). 25000 cells cm-2 HUVEC were seeded and grown for 24h. Silencing was performed following manufacturer's instructions, using a fixed amount of TFRC siRNA and of oligofectamine transfection reagent (1x corresponding to 10 pmol siRNA and 1µl oligofectamine per well) for 24, 48 or 72h (a) or with increasing amounts of TFRC siRNA and transfection reagent (1x: 10 pmol siRNA and 1µl oligofectamine; 2x: 20 pmol siRNA and 2µl oligofectamine; 3x: 30 pmol siRNA and 3µl oligofectamine) for 72 hours (b) Silencing was also performed on other CME targets for 48h with a fixed amount of siRNA and transfection reagent (2x: 20 pmol siRNA and 2µl oligofectamine) (c). Cells exposed to a negative siRNA in the same conditions were used as control. After silencing, cells were exposed to 15 µg ml-1 red fluorescent transferrin (TFR) in serum free medium for 10 minutes and their fluorescence measured by flow cytometry. The results are the averaged median intensity and standard deviation over three replicates, normalized by the results in control cells. In all cases transferrin uptake was reduced to a maximum of 50-60% in cells silenced for TFR in comparison to control cells, while up to 90% reduction can be obtained with the same method in cancer cells such as HeLa (data not shown). TFR uptake was barely affected in cells silenced for CME targets. This indicated low silencing efficacy in primary cells, in agreement with results in literature.

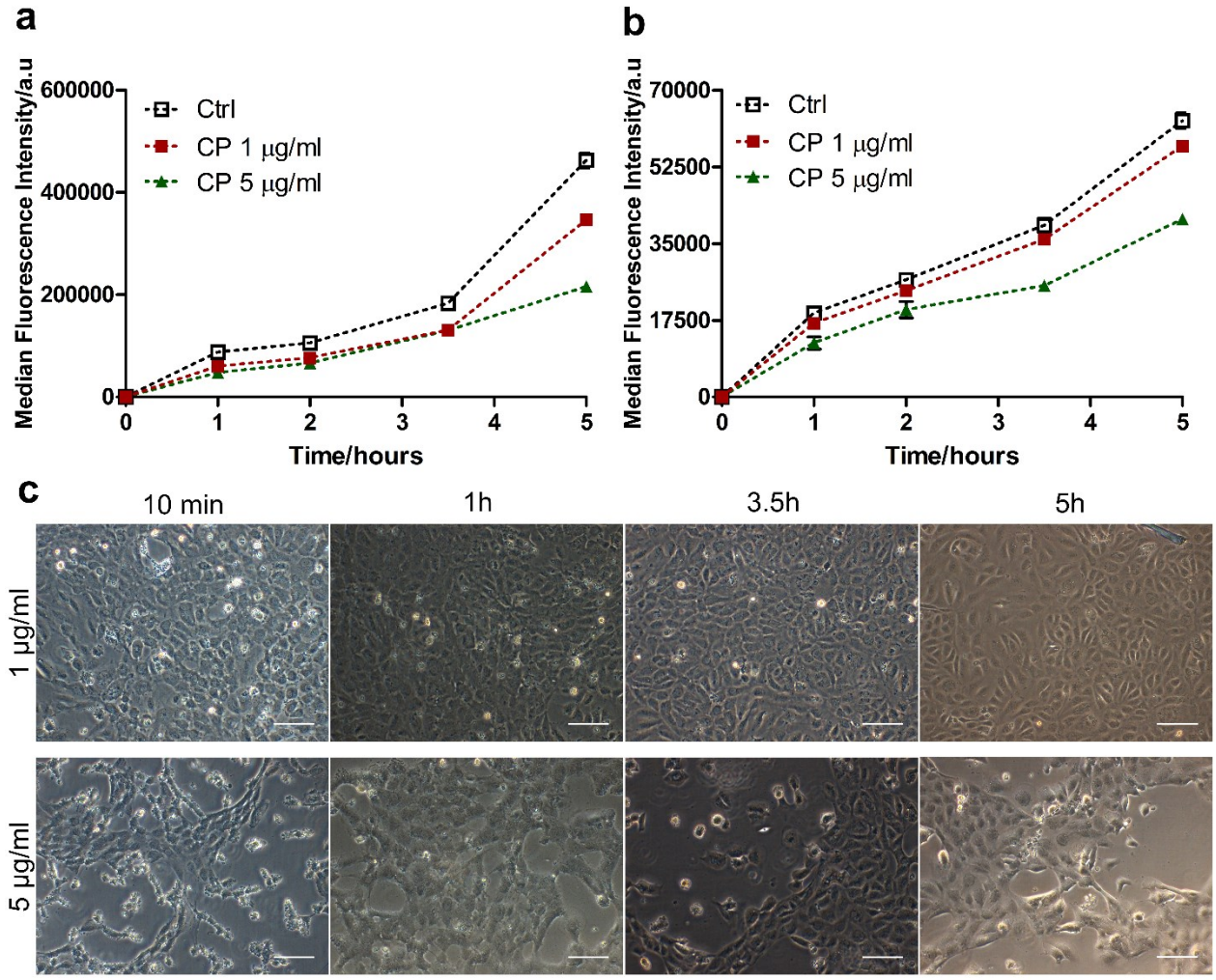

Figure S17. Optimization of chlorpromazine (CP) dose on HUVEC barriers. HUVEC barriers (seven days after seeding 3000 cells cm-2) were exposed to 1 or 5 µg ml-1 CP. Efficacy of CP (a) and effect of CP on nanoparticle uptake (b) were assessed by measuring the uptake of 2 µg ml-1 BODIPY LDL and 100 µg ml-1 50 nm red SiO2 nanoparticles in EBM2 supplemented with 4 mg ml-1 human serum, respectively, for the indicated doses and times in the presence or absence of CP. Results are the average and standard deviation of three replicates. Light microscopy images of HUVEC barriers (c) were taken to monitor the effect of CP on HUVEC barrier integrity after exposure for the indicated times to the different CP doses (scale bar: 100 µm). The results showed that in all conditions tested, exposure to CP resulted in loss of barrier integrity. Furthermore, at the lower dose tested, CP efficacy in blocking LDL uptake was minimal. Thus, 5 µg ml-1 CP was selected for further experiments on cell barriers, to ensure at least a partial inhibition, even if this dose led inevitably to loss of barrier integrity.

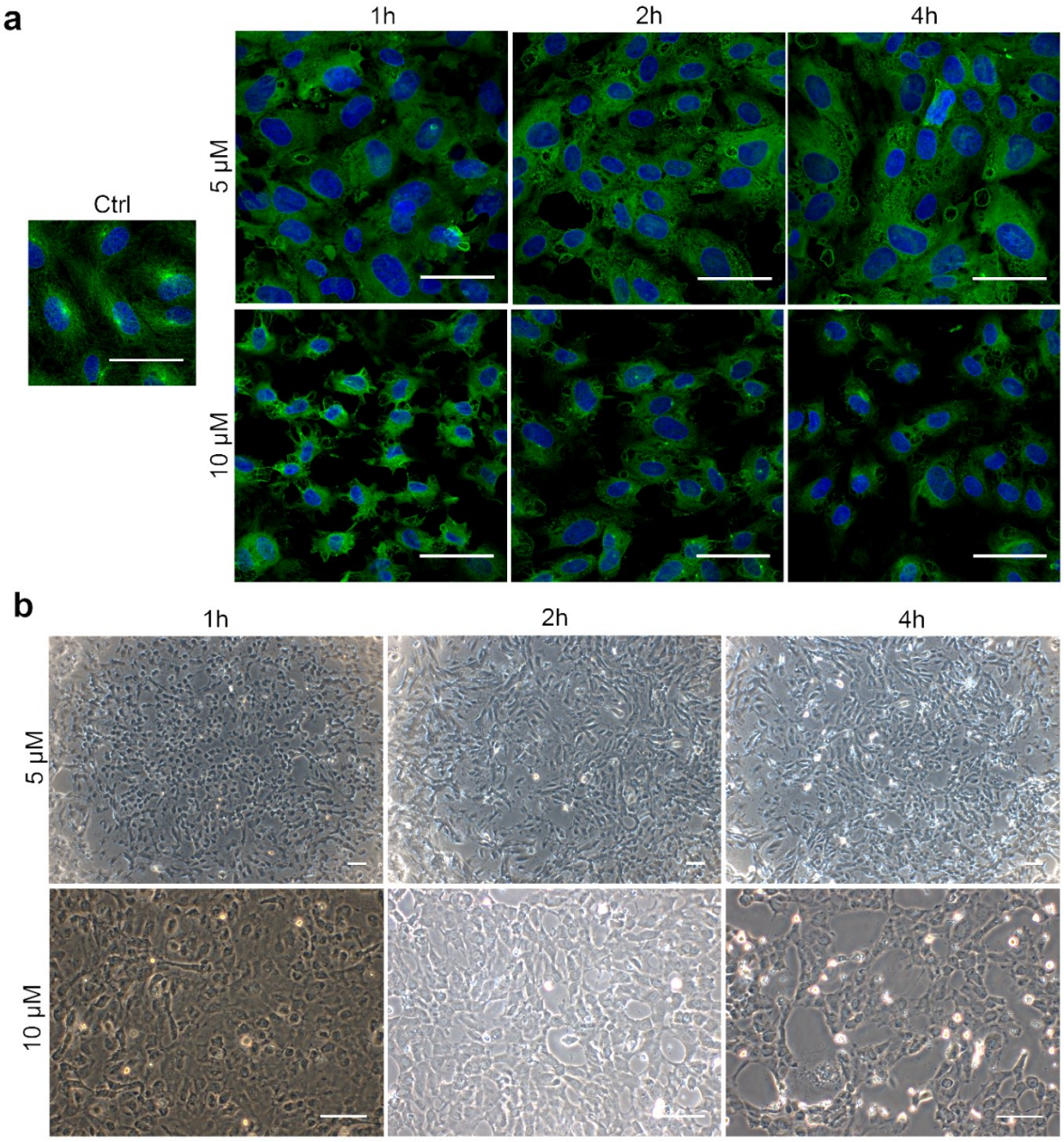

Figure S18. Optimization of nocodazole (NZ) dose on HUVEC barriers. HUVEC barriers (seven days after seeding 3000 cells cm-2) were exposed to 5 or 10 µM NZ. (a) Confocal images after staining the cells with fluorescent antibodies against tubulin were taken on untreated control barriers (Ctrl) and barriers exposed to the different doses of NZ for the indicate times (scale bar: 50 µm). Light microscopy images of HUVEC barriers (b) were taken after exposure for the indicated times to the different NZ doses to monitor the effect on HUVEC barrier integrity (scale bar: 100 µm). The results showed that even at the lower dose tested, exposure to NZ led to loss of barrier integrity. It is likely that loss of microtubules as induced by this compound leads inevitably to loss of barrier integrity (the tested doses are already much lower than what usually applied for this kind of compounds).[36]

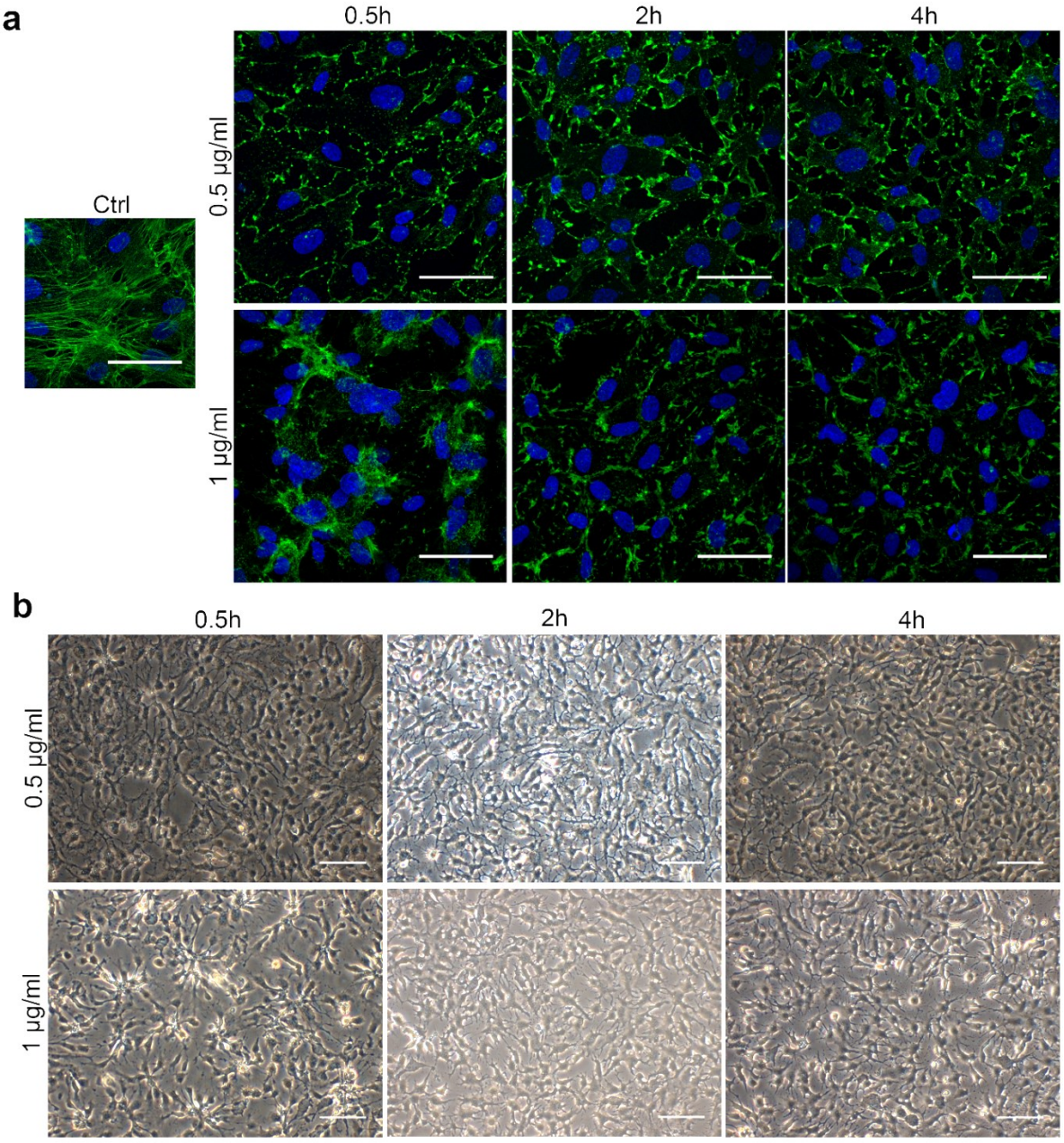

Figure S19. Optimization of cytochalasin D (CytoD) dose on HUVEC barriers. HUVEC barriers (seven days after seeding 3000 cells cm-2) were exposed to 0.5 or 1 µg ml-1 CytoD. (a) Confocal images after actin staining (performed as described in the Experimental Section) were taken on untreated control barriers (Ctrl) and barriers exposed to the different doses of CytoD for the indicated times (scale bar: 50 µm). Light microscopy images of HUVEC barriers (b) were taken after exposure for the indicated times to the different CytoD doses to show the effect on HUVEC barrier integrity (scale bar: 100 µm). The results showed that even at the lower dose tested, exposure to CytoD led to loss of barrier integrity. It is likely that loss of actin as induced by this compound leads inevitably to loss of barrier integrity (the tested doses are already much lower than what usually applied for this kind of compounds).[36]

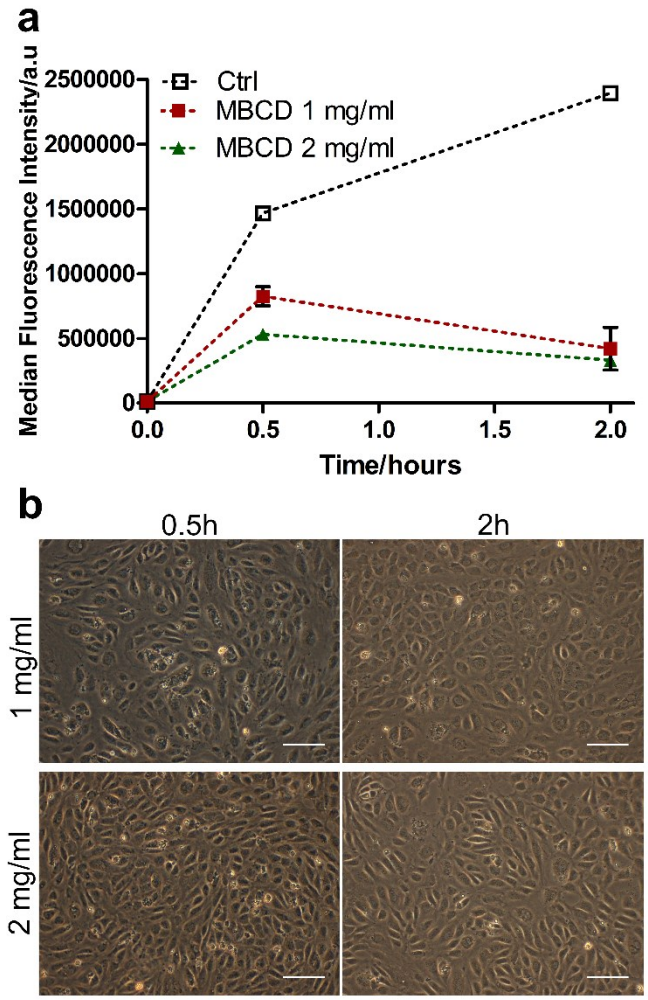

Figure S20. Optimization of methyl-β-cyclodextrin (MBCD) dose on HUVEC barriers. HUVEC barriers (seven days after seeding 3000 cells cm-2) were exposed to 1 or 2 mg ml-1 MBCD. Efficacy of MBCD (a) was assessed by measuring the uptake of 1 µg ml-1 BODIPY LacCer for the indicated doses and times in the presence or absence of MBCD. Results are the average and standard deviation of three replicates. Light microscopy images of HUVEC barriers (b) were taken after exposure for the indicated times to the different MBCD doses to monitor the effect on HUVEC barrier integrity (scale bar: 100 µm). The results showed that in all conditions tested MBCD efficacy in blocking LacCer uptake was optimal, and barrier integrity was maintained.

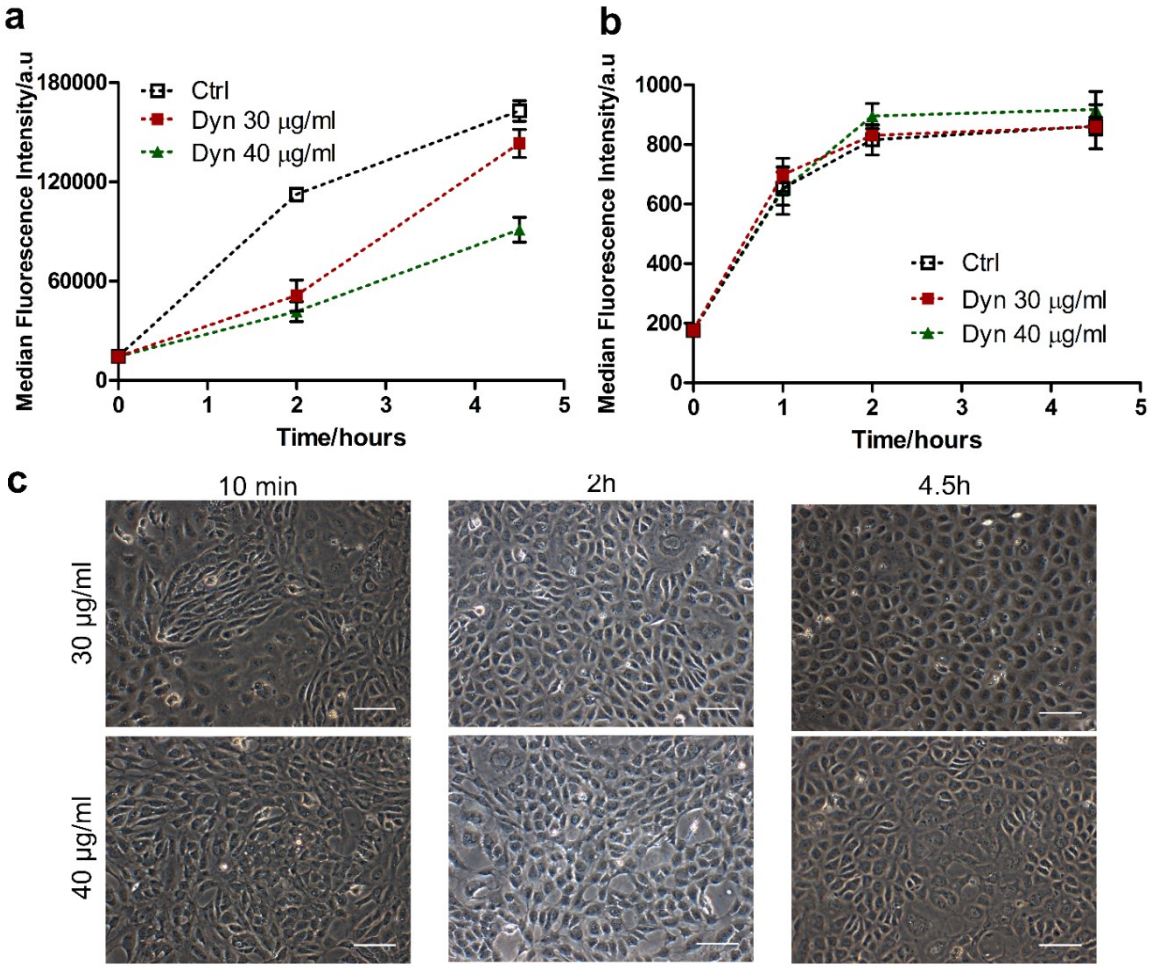

Figure S21. Optimization of dynasore (Dyn) dose on HUVEC barriers. HUVEC barriers (seven days after seeding 3000 cells cm-2) were exposed to 30 or 40 µg ml-1 Dyn. Efficacy of Dyn (a) and effect of Dyn on nanoparticle uptake (b) were assessed by measuring the uptake of 2 µg ml-1 BODIPY LDL and 100 µg ml-1 50 nm red SiO2 nanoparticles in EBM2 supplemented with 4 mg ml-1 human serum, respectively, in the presence or absence of Dyn. Results are the average and standard deviation of three replicates. Light microscopy images of HUVEC barriers (c) were taken after exposure for the indicated times to the different Dyn doses to monitor the effect on HUVEC barrier integrity (scale bar: 100 µm). The results showed that in all conditions tested Dyn efficacy in blocking LDL uptake was high, and barrier integrity was maintained.

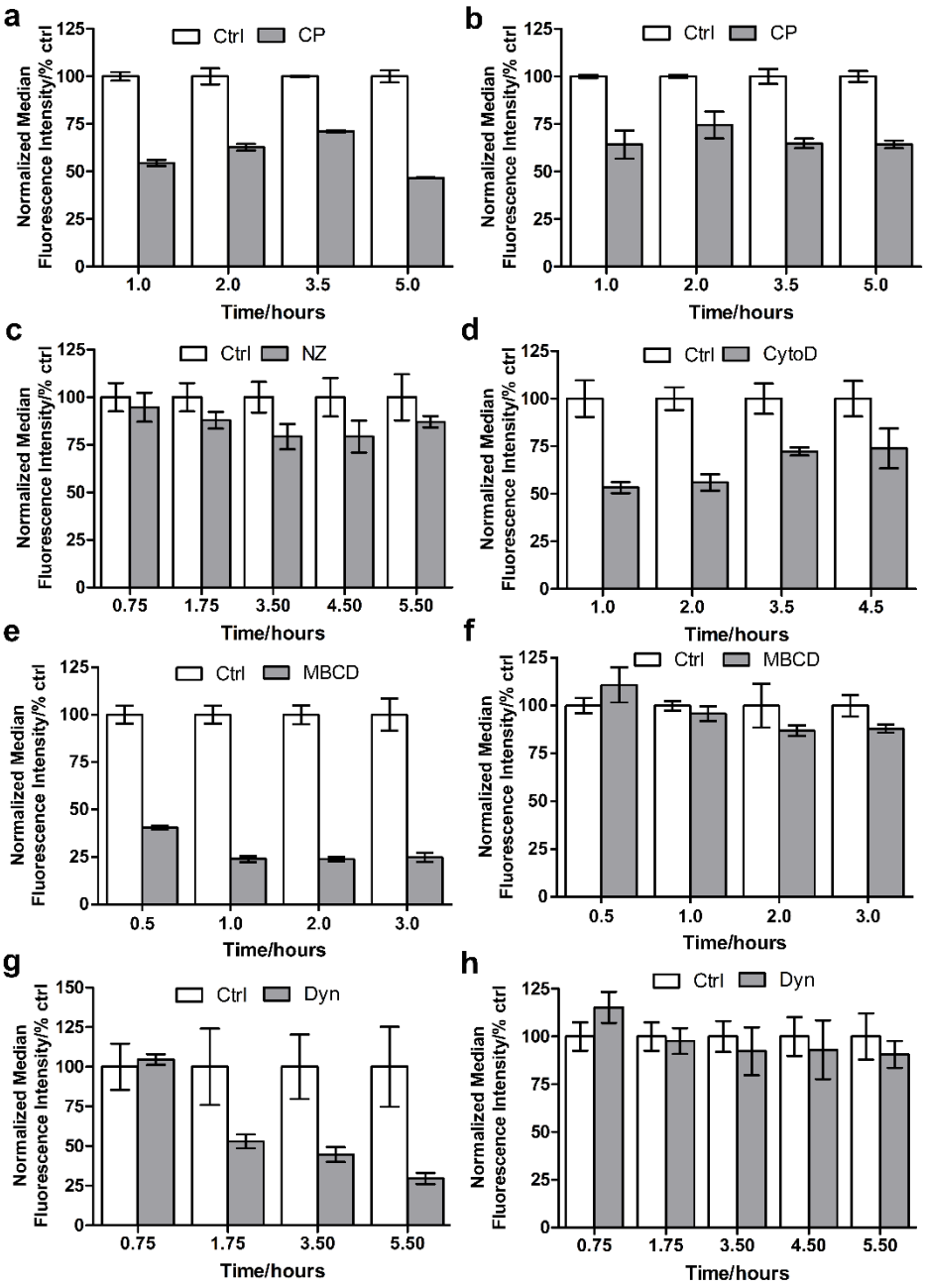

Figure S22. Normalized uptake levels in HUVEC barriers exposed to different inhibitors. The same data of Figure 4 are shown here after normalization for the uptake in control cells without inhibitors. HUVEC barriers (seven days after seeding 3000 cells cm-2) were exposed to 5 µg ml-1 chlorpromazine (CP) (a and b), 5 µM nocodazole (NZ) (c), 0.5 µg ml-1 cytochalasin D (CytoD) (d), 2 mg ml-1 methyl-β-cyclodextrin (MBCD) (e and f), or 30 µg ml-1 dynasore (Dyn) (g and h). Left panels (a, e and g): uptake by flow cytometry of 2 µg ml-1 BODIPY LDL (a and g), and 1 µg ml-1 of BODIPY LacCer (e) in control cells (Ctrl) and cells exposed to chlorpromazine, dynasore and MβCD respectively, as a control for drug efficacy. Right panels (b, d, f and h) and c: effect of the drugs on nanoparticle uptake. HUVEC barriers were exposed to 100 µg ml-1 50 nm red SiO2 nanoparticles in EBM-2 supplemented with 4 mg ml-1 human serum for the indicated times in the presence or absence of the different drugs. The results are the average and standard deviation of three replicates, normalized by the uptake in control cells without inhibitors.

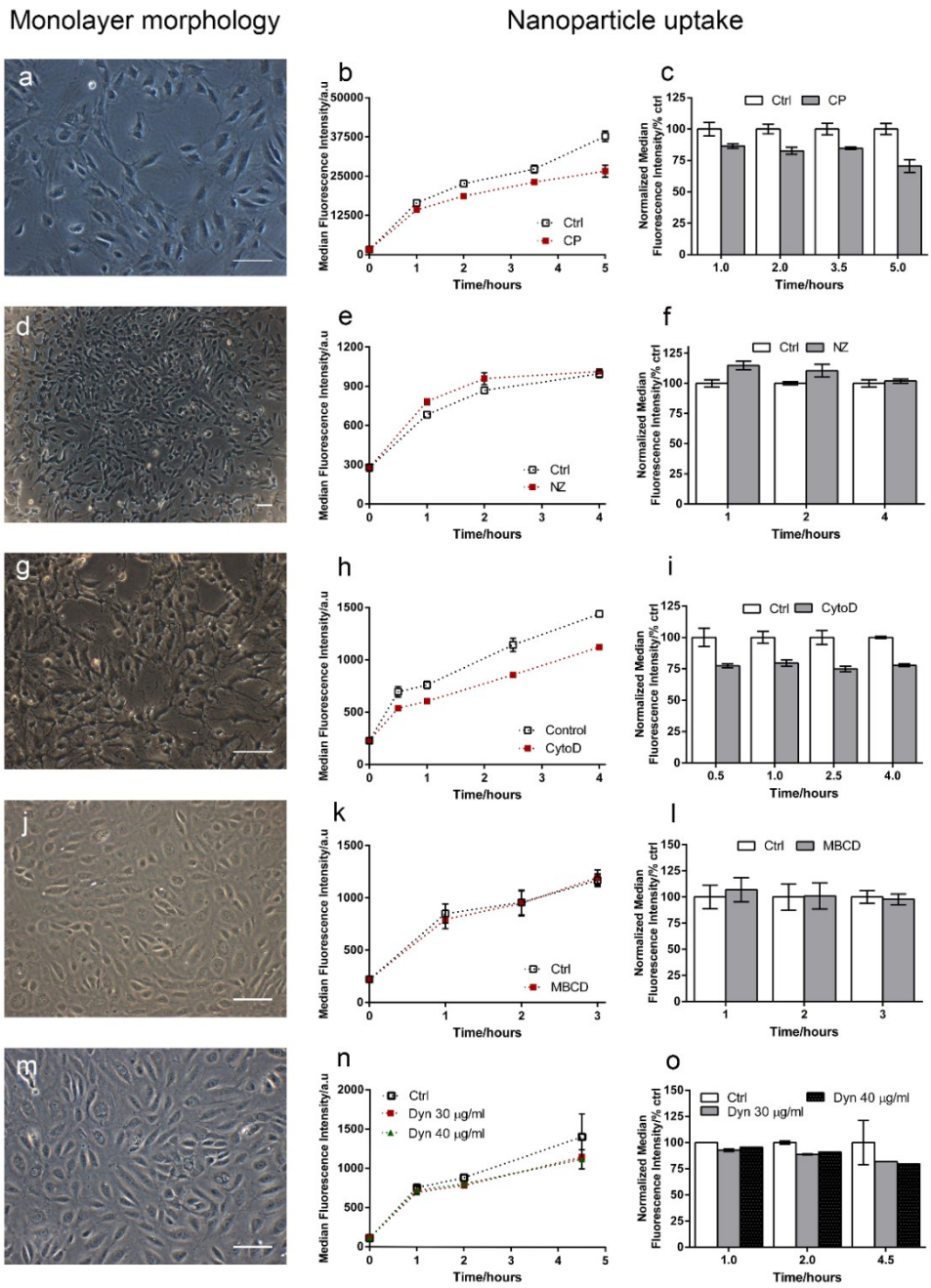

Figure S23. Uptake mechanisms in confluent HUVEC cells. Confluent HUVEC cells (one day after seeding 25000 cells cm-2) were exposed to 5 µg ml-1 chlorpromazine (CP) (a-c), 5 µM nocodazole (NZ) (d-f), 0.5 µg ml-1 cytochalasin D (CytoD) (g-i), 2 mg ml-1 methyl-β-cyclodextrin (MBCD) (j-l), or 30 µg ml-1 dynasore (Dyn) (m-o). Left panels: light microscopy images of confluent HUVEC cell morphology after exposure to each inhibitor (scale bar: 100 µm). Middle panels: effect of the inhibitors on nanoparticle uptake. Confluent HUVEC cells were exposed to 100 µg ml-1 50 nm SiO2 nanoparticles in EBM-2 supplemented with 4 mg ml-1 human serum for the indicated times in the presence or absence (Ctrl) of the different inhibitors. Results are the average and standard deviation of three replicates. Right panels: the same nanoparticle uptake results, normalized for uptake levels in control cells without inhibitors.